Ultrasound-enhanced zero-valent copper activation of persulfate for the degradation of Bisphenol AF

Qun Wang, Ye Cao, Han Zeng, Youheng Liang, Jun Ma, Xiaohui Lu

PII: S1385-8947(19)31537-2
DOI: https://doi.org/10.1016/j.cej.2019.122143
Article Number: 122143
Reference: CEJ 122143

To appear in: *Chemical Engineering Journal*

Received Date: 29 March 2019
Revised Date: 21 June 2019
Accepted Date: 2 July 2019

Please cite this article as: Q. Wang, Y. Cao, H. Zeng, Y. Liang, J. Ma, X. Lu, Ultrasound-enhanced zero-valent copper activation of persulfate for the degradation of Bisphenol AF, *Chemical Engineering Journal* (2019), doi: https://doi.org/10.1016/j.cej.2019.122143

Ultrasound-enhanced zero-valent copper activation of persulfate for the degradation of Bisphenol AF

Qun Wang[a,*], Ye Cao[a], Han Zeng[a], Youheng Liang[a], Jun Ma[b], Xiaohui Lu[b,*]

[a] *Faculty of Geoscience and Environmental Engineering, Southwest Jiaotong University, Chengdu 610031, P.R. China*

[b] *State Key Laboratory of Urban Water Resource and Environment, Harbin Institute of Technology, Harbin 150090, P.R. China*

* *Corresponding author.*

Tel: +86 18215559048 E-mail: xhlu_swjtu@126.com (Q. Wang);

Tel: +86 15202890282; E-mail: luxiaohuihit@163.com (X. Lu).

Abstract

Ultrasound (US) was introduced into a persulfate (PS) / zero-valent copper (ZVC) system for the degradation of bisphenol AF (BPAF). In this system, ZVC worked as a catalyst to activate PS. Compared with the PS/ZVC process, the degradation rate of BPAF in the PS/ZVC/US system raised significantly from 59.8% to 97.0% due to a synergistic interaction between sonolysis and a heterogeneous reaction. When ultrasound was 120 W at 20 kHz and initial BPAF concentration was 20 μmol/L, the BPAF could be completely removed after a 60-min reaction with 0.5 g/L ZVC, 1 mM PS. According to kinetics research, the decomposition of BPAF in a PS/ZVC/US system could be separated into two stages with a demarcation point after about 20 min of reaction via pseudo-first-order rate constants (k_{obs}). A Quantitative analytical

modeling for the study of main radicals was established, and the result indicated $SO_4^{\cdot-}$ was the predominant radical in acidic conditions and both ·OH and $SO_4^{\cdot-}$ were the predominant radicals in relative basic conditions. Moreover, the effects of initial persulfate dosage, initial BPAF concentration, and coexisting inorganic anions on BPAF degradation were evaluated. A high-accuracy mass spectrometer was used to study the oxidation process and potential activities were deduced. Finally, the possible reaction mechanisms in the PS/ZVC/US system is proposed that the surface heterogeneous catalysis was the key step to activate PS. This work will promote the understanding of the utilization of ZVC in advanced oxidation and also the key role of Cu^+ in activating PS.

Keywords: Bisphenol AF; Persulfate; Zero-valant copper; Kinetics study; Degradation pathways; Free radicals

1 Introduction

Bisphenol, a big group of chemicals, is mainly applied for improving the translucence, mechanical behavior, and circuit performance of industrial products [1]. Bisphenol A (BPA), of which millions of tons are used every year, is among the most frequently abused bisphenols in everyday applications such as thermal paper, plastics, cans and dental sealants [2]. However, scientific research has confirmed that BPA could be harmful to organisms, especially in the reproductive tract and in embryonic development [3, 4]. Bisphenol AF (BPAF) is another material whose construction is analogous to BPA (Fig. 1). It is clear that the difference between BPA and BPAF is in their functional groups that a CF_3 group takes the place of a methyl group bonded to the central bridging carbon atom in BPA to form BPAF. This could assist to improve the thermal and chemical stability of this compound [5]. Therefore, BPAF is commonly adopted as a BPA substitute for the production of polycarbonates, polyamides, and polyesters [6]. Unfortunately, recent studies demonstrate that BPAF also displays endocrine disrupting effects [7, 8], and it has been found in different environmental matrices. For instance, it has been detected at up to 15.3 μg/L in rivers, 0.2 μg/g dry weight in sediment, 0.739 μg/g dry weight in indoor dust, and 0.3 ng/L in well water [5]. In addition, trace BPAF also appears in foodstuffs [9], fetal cord blood [10] and urine samples [11]. More importantly, BPAF is easier to accumulate in an organism [12] and is harder to degrade than BPA [13], indicating BPAF could possibly exist in the environment for a long time and create more environmental issues. Therefore, it is urgently needed to remove BPAF from potable water, drainage,

and river systems.

Recent research has confirmed advanced oxidation processes (AOPs) is an effective way to degrade organic material in liquids through the formation of strong oxidants like hydroxyl radical (·OH) and sulfate radical ($SO_4^{\cdot-}$) [14]. Among them, ·OH is the main oxidant in traditional AOPs, which could oxidize a wide range of organic contaminants non-selectively, and the $SO_4^{\cdot-}$ has attracted much interest especially for in situ chemical oxidation [15-17]. Regarding ·OH, E. Nikfar et al. Employed ultrasound along with hydrogen peroxide for the removal of BPA from aqueous solutions. They found that the degradation of BPA was enhanced using a process combining ultrasonic radiation with hydrogen peroxide due to a large number of ·OH radicals produced by cavitation in the presence of hydrogen peroxide [18]. In addition to ·OH, $SO_4^{\cdot-}$ is gaining more consideration due to its selective oxidation capability and higher redox potential within a wider pH range (E^0 ($SO_4^{\cdot-}$) = 2.5 V - 3.1 V in both alkali and acidic condition; E^0 (·OH) = 1.8 V in alkali condition and 2.7V in acidic condition) [19-21]. $SO_4^{\cdot-}$ is generated mainly via persulfate (PS, $S_2O_8^{2-}$) and peroxymonosulfate (PMS, HSO_5^-) activation with catalysts like heat [22], UV radiation [16, 23, 24], transition metals [25-28], ultrasound [29-31], base [32], and activated carbon [33]. Similar to ·OH, the mechanism of $SO_4^{\cdot-}$ reacting with organics may involve electron mobility, hydrogen extraction, and addition mechanisms. Nevertheless, $SO_4^{\cdot-}$ reacts more selectively via electron transfer [34] and thus $SO_4^{\cdot-}$ would be affected less by degradation byproducts and natural organic matter during oxidation, especially when degrading aromatics. Besides, handling of

$S_2O_8^{2-}$ is much easier than handling H_2O_2, and also exhibits a better stability and shows a limited loss in use at a low cost [20].

Sono-activated persulfate is effective in decomposing many pollutants in liquids [29]. The role of ultrasound is to produce ·OH by cavitation [18]. However, for many ultrasound-based water treatment technics, the costs for purification were unsatisfactory due to the utilization efficiency of ultrasound was too low when ultrasound was used alone [35]. In recent years, many scholars have proposed to combine ultrasound with AOPs to enhance the utilization efficiency of ultrasound. Xiaoyan et al. used nanosized zero-valent copper (nZVC) to activate H_2O_2 to remove norfloxacin, and a significant enhanced removal rate was obtained when ultrasound was introduced [30]. This phenomenon could be attributed to the fact that the corrosion of metal catalysts can be strengthened significantly by better cleaned surfaces of catalysts in the presence of ultrasound, which accelerates the catalytic reaction [36]. It is well-known that like H_2O_2, PS can be also activated by metal catalysts. Peng et al. investigated the oxidation of 2,4-dichlorophenol in a PS/nZVC system and in analogous systems. The results revealed that both PS and PMS could accelerate the decomposition of ZVC or nZVC, as well as to stimulate Cu^+, which decomposes PS or PMS, to generate ·OH and $SO_4^{\cdot-}$ [26]. Some other researchers investigated PS activation process involving CuS and they found that the activation site mainly occurred on the surface of CuS [27]. This conclusion suggested ultrasound had the ability to strengthen the heterogeneous activation process of PS with metal as the catalyst through mass transfer effect and mechanical effect. Through these two

effects, ultrasound could continuously remove the activation and oxidation residues during the reaction and enhance the activation. However, no study has reported the removal efficiency and mechanisms of organic contaminants in the PS/ZVC system with introduce of ultrasound.

The major objectives of this work are (1) to investigate the decomposition efficiency of BPAF in a PS/ZVC/US system compared with PS, US, ZVC, PS/US, PS/ZVC, and ZVC/US systems; (2) to quantify the contribution of BPAF degradation involving $\cdot OH$ and $SO_4^{\cdot-}$ at different pH conditions and develop a pseudo-first-order model to determine kinetics parameters in the oxidation of BPAF during a PS/ZVC/US process; (3) to evaluate the effect of various oxidant dosages, initial target contaminant concentrations, and coexisting anions on degradation efficiency via the pseudo-first-order model developed in (2); (4) to analyze the oxidation products by using a high performance liquid chromatography/electrospray ionization-triple quadrupole mass spectrometer (HPLC/ESI-QQQ), and propose the degradation pathways of BPAF; and (5) to suggest possible degradation mechanisms of the oxidation of BPAF and the role of ultrasound in a PS/ZVC/US system.

2 Materials and methods

2.1 Chemicals

ZVC (≥99.99%, 325 meshes), neocuproine hemihydrate (NP, ≥98%), BPAF (≥98%) and potassium persulfate were provided by Aladdin Industry Corporation (Shanghai, China). High-purity (≥99.99%) methanol of HPLC grade was obtained

from Fisher Chemical (Shanghai, China). Anhydrous methanol (≥ 99.5%) was obtained from Kelong Chemical (Chengdu, China). Other chemicals used in various procedures such as KI, HNO_3, NaOH, $NaHCO_3$, NaCl, $NaNO_3$, Na_2SO_4 and $CuSO_4$ were provided by Sinopharm Chemical Reagent Co. Ltd., (Shanghai, China). All the reagents were selected strictly to ensure high purity. To satisfy the high-purity demand, water used in this work was processed by a filter system (Ulupure, China).

2.2 Instruments and methods

To test the properties of catalyst to degrade chemicals, the analysis was executed in an ultrasonic processor (JY92-2D, Scientz, China) at a frequency of 20 kHz, and the output power was set between 60 and 960 W. An ultrasonic detector was immersed in a container with 100 mL BPAF, which was obtained by mixing high-purity water for 48 h using a magnetic agitator (JB-2, Leici, China). In addition, to keep the temperature around 20± 1 ℃, the glass beaker was placed in an ice bath, with continuous circulating water from a low-temperature thermostat bath. As needed, HNO_3 or NaOH solutions were employed to adjust the pH, monitored by a pH-meter (PHB-4, Leici, China). The stock solution of BPAF (200 μM) and PS (100 mM) were prepared in advance. All physiochemical properties of BPAF are shown in Table 1. In terms of the degradation test, certain amount of ZVC and PS were added, followed immediately by an ultrasonic irradiation for 60 min. Of note, due to the fact that the degradation of BPAF could be negligible when only PS in the system (see Fig. 2), PS was added before the reaction began. After PS was added, the pH values would be

adjusted to around 4.0 as the initial pH, and then turned on the ultrasonic processor and added ZVC simultaneously to start the reaction. At times of 0, 2, 5, 10, 15, 20, 25, 30, 45 and 60 min, samples of 1-mL were collected and filtered by a polyether sulfone film (PES, 0.22 μm) for HPLC analysis, and certain volumes of sample were also withdrew for other analysis if necessary. Reactions were quenched by introducing 0.1 mL of anhydrous methanol into the samples. All tests were repeated, and average data were obtained.

2.3 Experimental analysis

Concentrations of BPAF, after being treated, were analyzed by a high performance liquid chromatograph (HPLC, Waters 2695, USA) equipped with a Waters 2996 diode array detector (DAD). A C18 column (5 μm, 4.6× 150mm, Waters, USA) preserved at 30 ℃ was employed for analysis. Methanol and ultrapure water (75: 25, v/v), in the mobile phase, were set to a flow rate of 1 $mL \cdot min^{-1}$. 20 μL of liquid was injected, while the DAD wavelength was tuned to 280 nm.

Potassium iodide method [37] was introduced for measuring the concentration of PS. PS could react with KI to form a yellow solution and its absorbance was 354 nm, which could be detected by an UV-vis spectrophotometer (UV4802, Unic instruments Co., Ltd, China). The stock solution was prepared in advance and used within 48 h.

A high performance liquid chromatography/electrospray ionization-triple quadrupole mass spectrometer (HPLC/ESI-QQQ, 5500 MS, ABSciex USA) was selected to identify the byproducts of the reaction. HPLC separation was conducted in an Agilent

Poroshell 120 EC-C18 column with dimensions of 3.0× 50 mm and 2.7 μM. Two phases (water and acetonitrile) composed the mobile phase, and they flowed at 0.2 mL per minute. The gradient was increased to 95% B in the first 10 min, kept at that value for 40 min, and then adjusted to the initial condition (5% B), for 10 min to reach the state of re-equilibration. Electrospray ionization (ESI-) at negative mode was employed to examine the mass spectra from 40 to 1000 m/z. As for the ion source, the ion spray was set at a floating voltage of 4500 V, source temperature was 500 ℃, curtain flowed at 35 psi, nebulizer was set at 50 psi, de-clustering potential (DP) was at -100 V and collision energy (CE) was set at -30-40 V, as described in a previous study [38].

The concentration of Cu^{2+} was measured by the L-ascorbic acid method [26]. The Cu^{2+} in solution could be reduced to Cu^{+} and chelated with NP to form a complex compound, which could be detected by an UV-vis spectrophotometer at 454 nm. The concentration of F^{-} was detected by an ion chromatography (IC 6000, wayeal Co., Ltd China) and TOC was measured by a TOC analyser (Multi N/C 2100, Analytik Jena, Germany).

2.4 Quantitative analytical modeling for PS/ZVC/US system

To determine the main radicals contributing to BPAF degradation, as well as to study the primary reactions at different pH values, a radical scavenger and a chemical probe were used in this experiment. As described in eqs. (1) and (2) [33], the reaction rate between TBA and ·OH follows a second-order constant, which is almost one

thousand times faster than that between TBA and $SO_4^{\cdot-}$.

$$t\text{-}BuOH + \cdot OH \rightarrow \text{intermediates}, \qquad k = (3.8-7.6)\times 10^8\ M^{-1}s^{-1} \tag{1}$$

$$t\text{-}BuOH + SO_4^{\cdot-} \rightarrow \text{intermediates}, \qquad k = (4.0-9.1)\times 10^5\ M^{-1}s^{-1} \tag{2}$$

According to previous research, having different activities of TBA with ·OH and $SO_4^{\cdot-}$. is a characteristic property that distinguishes the prevailing radicals in different chemical systems [39]. However, this method can only identify the predominant radical species qualitatively. In order to further investigate the action mechanism of radicals in a PS/ZVC/US system, a new mathematical model is proposed to determine the predominant radical species quantitatively.

Nitrobenzene (NB) is one of chemical probes that could be used to differentiate between the competitive kinetics of ·OH and $SO_4^{\cdot-}$ [40]. The decomposition of NB and BPAF can be described with second-order kinetics, as shown in eqs (3) and (4), separately.

$$-d[NB]/dt = k_{\cdot OH,NB}[NB][\cdot OH] \tag{3}$$

$$-d[BPAF]/dt = k_{\cdot OH,BPAF}[BPAF][\cdot OH] + k_{SO_4^{\cdot-},BPAF}[BPAF][SO_4^{\cdot-}] \tag{4}$$

In these equations, $k_{\cdot OH,NB}$ represents the constant of the second-order rate between the reaction of ·OH and NB, while $k_{\cdot OH,BPAF}$, $k_{SO_4^{\cdot-},BPAF}$ determined in Text S1, are the second-order rate constants for reactions of BPAF with ·OH and $SO_4^{\cdot-}$. The reaction between NB and $SO_4^{\cdot-}$ is very weak due to its low reaction rate constant (

$k_{SO_4^{\cdot-},NB} \leq 10^6\ M^{-1}s^{-1}$ [41]).

Rearrangement and integrating eqs. (3) and (4) lead to

$$\ln([NB]_t/[NB]_0) = -k_{\cdot OH,NB}\int[\cdot OH]dt \quad (5)$$

$$\ln([BPAF]_t/[BPAF]_0) = -(k_{\cdot OH,BPAF}\int[\cdot OH]dt + k_{SO_4^{\cdot-},BPAF}\int[SO_4^{\cdot-}]dt) \quad (6)$$

where $\int[\cdot OH]dt$ (namely, ·OH exposure) and $\int[SO_4^{\cdot-}]dt$ (namely, $SO_4^{\cdot-}$ exposure) are the time-integrated concentrations of ·OH and $SO_4^{\cdot-}$, respectively.

Dividing eq. (5) by eq. (6) leads to

$$\ln([BPAF]_t/[BPAF]_0) = (k_{SO_4^{\cdot-},BPAF}\int[SO_4^{\cdot-}]dt/\int[\cdot OH]dt + k_{\cdot OH,BPAF})\ln([NB]_t/[NB]_0)/k_{\cdot OH,NB} \quad (7)$$

A term R_{ct} is the proportion between $SO_4^{\cdot-}$ and ·OH exposures (eq. (8)) [42].

$$\int[SO_4^{\cdot-}]dt/\int[\cdot OH]dt = R_{ct} \quad (8)$$

R_{ct} can be obtained from the slopes of curves in graphs of $\ln([BPAF]_0/[BPAF]_t)$ vs $\ln([NB]_0/[NB]_t)$.

The contribution of oxidation of BPAF by ·OH and $SO_4^{\cdot-}$ can be calculated by using

$$f_{\cdot OH,BPAF} = k_{\cdot OH,BPAF}\int[\cdot OH]dt/(k_{\cdot OH,BPAF}\int[\cdot OH]dt + k_{SO_4^{\cdot-},BPAF}\int[SO_4^{\cdot-}]dt) \quad (9)$$

$$f_{SO_4^{\cdot-},BPAF} = k_{SO_4^{\cdot-},BPAF}\int[SO_4^{\cdot-}]dt/(k_{\cdot OH,BPAF}\int[\cdot OH]dt + k_{SO_4^{\cdot-},BPAF}\int[SO_4^{\cdot-}]dt) \quad (10)$$

Substitution of eq. (8) into eqs. (9) and (10) yields

$$f_{\cdot OH,BPAF} = k_{\cdot OH,BPAF}/(k_{\cdot OH,BPAF} + k_{SO_4^{\cdot-},BPAF}R_{ct}) \quad (11)$$

$$f_{SO_4^{\cdot-},BPAF} = k_{SO_4^{\cdot-},BPAF}/(k_{\cdot OH,BPAF}/R_{ct} + k_{SO_4^{\cdot-},BPAF}) \quad (12)$$

If the ratio of $f_{SO_4^{\cdot-},BPAF}$ to $f_{\cdot OH,BPAF}$ (eq. (13)) is greater than one, $SO_4^{\cdot-}$ is the

dominant radical.

$$f_{SO_4^{\cdot-},BPAF}/f_{\cdot OH,BPAF} = R_{ct}k_{SO_4^{\cdot-},BPAF}/k_{\cdot OH,BPAF} \quad (13)$$

3 Results and discussion

3.1 Degradation efficiency of BPAF in the PS/ZVC/US system

Fig.2 shows the change of BPAF content in various systems after being treated for 60 min. No obvious degradation of BPAF was observed when using ZVC or PS alone, indicating that ZVC and PS do not adsorb or decompose BPAF efficiently under such acidic aqueous condition (initial pH 4.0) [25, 43]. In this process, a very low content (13.7%) of BPAF was oxidized under the effect of ultrasonic radiation because radicals like ·OH, ·O, and H· do not form significantly with the decomposition of water (eqs. (14) and (15)) [30]. A similar result was also observed in a US/ZVC system, where BPAF was removed at an efficiency of only 16.7%, indicating that no significant reaction happened between ultrasound and ZVC. The slight acceleration (31.7%) in the PS/US system is ascribed to the generation of sulfate radicals from persulfate anions (eq. (16)), implying that the quantity of reactive radicals was too low to make the reaction take place at a high speed without a catalyst [29]. Therefore, in order to decompose BPAF, oxidants and catalysts are necessary parts.

$$H_2O +))) \rightarrow \cdot OH + H\cdot \quad (14)$$

$$O_2 +))) \rightarrow 2\cdot O \quad (15)$$

$$S_2O_8^{2-} +))) \rightarrow 2SO_4^{\cdot-} \quad (16)$$

In the PS/ZVC system, BPAF was removed at a rate of 59.8 %, which is much higher

than using PS or ZVC alone. The possible reason is that in the presence of a catalyst, PS decomposed faster, so more $SO_4^{\cdot-}$ was formed [26]. The removal efficiency was up to 97.0% in the sono-advanced PS/ZVC process, indicating that a positive synergistic activity existed in the PS/ZVC/US system [30]. Compared with the PS/ZVC system, the use of ultrasound could possibly continuously clean the catalyst surface, and accelerate the formation of cavities [44]. Alternatively, the introduction of ZVC in the PS/US system could supply more spaces for the formation of cavitation bubbles, and ultrasound radiation could clear out the residues in ZVC for PS activation and BPAF oxidation, thus improving the degradation efficiency [45].

3.2 Influence of pH and investigation of main radicals

Acidity and basicity are very important parameters influencing chemical activity. In this work, pH has a critical influence on the degradation of BPAF, as displayed in Fig. 3. BPAF was removed significantly (97.0%) when pH was 4.0, which is more than at pH 5.0 (87.0%), pH 8.0 (82.7%), pH 6.0 (82.6%) and pH 7.0 (63.6%). No extreme basic condition was adopted in order to avoid the phenomenon that the dominant parameter activating PS was OH^- rather than ZVC [32]. Previous study of the PS/ZVC system has demonstrated that when pH was changed from 2.3 to 7.3, the ability of the system to remove pollutants decreased [26]. During the acid catalyzation at low pH, a large number of $SO_4^{\cdot-}$ could be formed, which could possibly accelerate the degradation of BPAF [46]. In our system, experimental results followed the same trend; the degradation of BPAF dropped with pH increasing from 4.0 to 7.0. More

cuprous ions (Cu^+)—strong activators of PS—dissolved from the ZVC surface through the reaction between hydrogen ions and copper at pH 4.0 than pH 7.0 (eqs. (17) and (18)) [26], thus hindering the decomposition of BPAF in relatively neutral environments. As shown in Table 2 and Fig. S6(b), the pH change during the reaction at initial pH 4.0 further supports the conjecture. Moreover, the suppressed BPAF degradation performance at higher initial pH could be ascribed to the fact that the free Cu^+ could be quenched very quickly by OH^-, as described in eqs. (19) and (20) [47]. As reported by Peng Z et al., the appearance of PS was favorable to the filtration of Cu^+ via eq. (21) [26]. The surface charge of ZVC is determined by pH_{PZC}. Copper is negatively charged when the pH is higher than pH_{PZC} and is positively charged otherwise. Hence, with pH increasing, the surface of copper particles will become negative and will repel $S_2O_8^{2-}$. That will slow down the corrosion of ZVC by $S_2O_8^{2-}$ [26].

$$2Cu + 2H^+ \rightarrow 2Cu^+ + H_2 \quad (17)$$

$$Cu^+ + S_2O_8^{2-} \rightarrow Cu^{2+} + SO_4^{\cdot-} + SO_4^{2-} \quad (18)$$

$$Cu^+ + OH^- \rightarrow CuOH\downarrow \quad (19)$$

$$2CuOH \rightarrow Cu_2O + H_2O \quad (20)$$

$$2Cu + S_2O_8^{2-} \rightarrow 2Cu^+ + 2SO_4^{2-} \quad (21)$$

However, the degradation rate of BPAF increased at pH 8.0. This discrepancy could be ascribed to the following fact:

The PS degradation rate constant could be divided into two stages with a demarcation point after about 5 min of reaction and thus a two-stage degradation of BPAF also

formed (see Text S2). As shown in Table 2, k_{obs_2} was larger than k_{obs_1} at pH 8.0, totally opposite to what is observed at lower pH values. One possible reason might be that more ·OH is generated with the introduction of ultrasound at higher pH values. Secondly, during this process, the decomposition of PS was more rapid at pH 8.0, indicating a strong base-catalyzed hydrolysis of PS happened, which leaded an enhanced activation effect (see Text S3 and Fig. S6). Thirdly, as pH increases, $SO_4^{\cdot -}$ will be exhausted by OH^- and transformed to ·OH, especially under strong alkaline conditions (eqs. (22) and (23) [28, 48]). Although ·OH decays more rapidly by nontarget species, its redox potential is higher than that of $SO_4^{\cdot -}$ at high pH values, and thus a higher degradation rate of BPAF was observed from pH 7.0 to pH 8.0.

$$SO_4^{\cdot -} + H_2O \rightarrow SO_4^{2-} + H^+ + \cdot OH \quad (22)$$

$$SO_4^{\cdot -} + OH^- \rightarrow SO_4^{2-} + \cdot OH \quad (23)$$

$$2S_2O_8^{2-} + 2H_2O \rightarrow O_2 + 4SO_4^{2-} + 4H^+ \quad (24)$$

In order to identify the main radicals contributing most to the degradation of BPAF at different pH values quantitatively, experiments with the addition of a chemical probe NB were conducted. As mentioned in Section 2.4, this process was employed to study the radical contribution for degradation of BPAF quantitively in PS/ZVC/US system by monitoring NB degradation. Curvilinear relationships on a logarithmic scale were observed between the degradation of BPAF and NB during the reaction (Fig. 4), indicating that the value R_{ct} was variable. The effect of pH value on the contribution of radicals to oxidation of contaminants could be assessed by the values of R_{ct}, $k_{\cdot OH,BPAF}$, and $k_{SO_4^{\cdot -},BPAF}$. Of particular note is that we only invoked the data

before 15 min of reaction for radical contribution analysis, because the degradation of BPAF and chemical probe would be greatly influenced by by-products after certain reaction time, and thus it was unsuitable to invoke it for further analysis. As shown in Fig. 5 and Table 3, In the acidic condition, $SO_4^{\cdot-}$ played a relatively important role for degradation of contaminants, and $SO_4^{\cdot-}$ contributed less in higher pH values due to the fact that the lack of H^+ would slow down the Cu^+ release, resulting in less $SO_4^{\cdot-}$ yields. Besides, as shown in Fig. S6(b), the pH value would be reduced as the reaction progresses when initial pH values were higher than 5.0, which could accelerate the erosion of ZVC, contributing to the generation of $SO_4^{\cdot-}$. The decrease of pH values could be ascribed to the weak hydrolysis of PS in water (eq. (24)) [49] and the base-catalyzed hydrolysis of PS as described in Text S3. In a relative basic condition, the value of $f_{SO_4^{\cdot-},BPAF}/f_{\cdot OH,BPAF}$ was closer to 1.0, indicating ·OH became the predominant oxidizer as well as the $SO_4^{\cdot-}$. This result could be ascribed to the fact that part of the $SO_4^{\cdot-}$ could transform to ·OH according to eq. (23), enhancing the contribution of ·OH to the degradation of BPAF. Previous research also reported a similar phenomenon [26]. Qualitative investigation with the introduction of a scavenger TBA was also conducted to verify the result (see in Text S4).

3.3 Influence of several key parameters

3.3.1 Influence of initial concentration of PS

Fig. 6 and Table 4 show how PS concentration influenced the degradation of BPAF. A higher initial concentration of PS led to a higher removal rate of BPAF. The

degradation of BPAF can be described by pseudo-first order kinetics during stage one. When initial PS concentration changed from 1 mM to 4 mM, the rate constants (k_{obs_1}) rose from 0.09782 min^{-1} to 0.16829 min^{-1}. BPAF was totally removed within 45, 25, and 20 min when the persulfate concentration was 2, 3, and 4 mM, respectively. No stage two was observed when initial persulfate concentration was 3 and 4 mM, as large amounts of radicals were yielded in stage one due to a high dosage of PS, which was enough to degrade almost all target contaminants existing in aqueous solutions. Several studies have shown that high oxidant dosage will reduce the degradation of target compounds [50], and it is generally believed that some reverse reactions, side reactions, and excessive oxidant (eqs. (25)-(28)) may lead a scavenging effect on $SO_4^{\cdot -}$ and ·OH [29, 51]. However, no inhibition was observed in the present study since the oxidant dosage was below the inhibition point.

$$S_2O_8^{2-} + \cdot OH \rightarrow OH^- + S_2O_8^{\cdot -} \quad (25)$$

$$S_2O_8^{2-} + SO_4^{\cdot -} \rightarrow SO_4^{2-} + S_2O_8^{\cdot -} \quad (26)$$

$$SO_4^{\cdot -} + SO_4^{\cdot -} \rightarrow S_2O_8^{2-} \quad (27)$$

$$S_2O_8^{2-} + 2 \cdot OH \rightarrow 2HSO_5^- \quad (28)$$

3.3.2 Influence of starting concentration of BPAF

The influence of the original BPAF concentration on BPAF degradation in PS/ZVC/US is shown in Fig. 7. As anticipated, higher concentration of the original BPAF led to less degradation of BPAF. The degradation rates for BPAF were 100%, 97.0%, 94.2%, and 87.3%, respectively, when the initial concentrations of BPAF were

10, 20, 30, and 40 μM. The BPAF degradation in this system at different starting concentrations was consistent with the pseudo-first-order kinetics model (Table 4). The rate constants in both stages showed a declining trend with a rise of the starting concentration of contaminants. This phenomenon could be explained as follows: First, BPAF was oxidized and decomposed by radicals, leading to the formation of abundant by-products. At a higher starting concentration of BPAF, a greater amount of by-products would take part in the reaction with active radicals, resulting in a decrease of the concentrations of $SO_4^{\cdot-}$ and ·OH. A similar trend was also observed in some analogous AOPs [31].

3.3.3 Influence of coexisting inorganic anions

By introducing inorganic anions with various concentrations, we could study how inorganic anions influence the degradation process. Fig. 8 displays the relationship of $[BPAF]_t/[BPAF]_0$ to different amounts of inorganic anions. As shown in the figure, the degradation rate of BPAF was 97.0% at initial pH 4.0 and 82.6% at initial pH 6.0 (for HCO_3^-) with no addition of inorganic anions. Degradation of BPAF was also influenced differently by different types of inorganic anions.

Because of the low rate constant between NO_3^- and $SO_4^{\cdot-}$ (5.0×10^4 $M^{-1}s^{-1}$), NO_3^- can only slightly influence the degradation of BPAF (Fig. 8(a)), which is consistent with our previous study [22]. As revealed in Fig. 8(b), the addition of SO_4^{2-} brought out a slight promotion when the initial SO_4^{2-} concentration was low. However, a lower contaminant removal was observed when the initial concentration of SO_4^{2-}

was increased. The BPAF removal efficiency decreased from 97.0% to 59.7% when 10 mM SO_4^{2-} was added to the PS/ZVC/US system. The positive impact of SO_4^{2-} on BPAF degradation can be explained on the basis of the salting-out effect of inorganic ions. Some researchers reported that sulfate ions cause high salting-out effect, and thus the solute was pushed towards the highly reactive interface region of the cavitation bubble to facilitate the degradation [52]. At the same time, a higher concentration of SO_4^{2-} produced secondary $SO_4^{\cdot-}$ through eq. (29).

$$SO_4^{2-} + \cdot OH \rightarrow H_2O + SO_4^{\cdot-} \quad (29)$$

$$Cu^{2+} + Cu \leftrightarrow 2Cu^{+} \quad (30)$$

High concentration of initial SO_4^{2-} might play a detrimental role in BPAF oxidation. Several researchers have studied the equilibrium concentration of Cu^{2+} in sulfate media. They reported that an equilibrium equation (eq. (30)) existed in solution and that the concentrations of Cu^{2+} and SO_4^{2-}, as well as temperature, had a significant effect on the equilibrium Cu^{+} concentration [53]. It is obvious that the optimum initial concentration of SO_4^{2-} for pollutant removal is about 0-1 mM in a PS/ZVC/US system. The reference [53] showed that the optimum concentration of sulfate anion that leaded a maximum salting-out effect was 100 ppm (about 1.042 mM in PS/ZVC/US system). This result was similar with our experimental observation that 1.0 mM sulfate anion had a positive influence on BPAF degradation.

Fig. 8(c) displays the double effect of Cl^- in the degradation process of BPAF. It can be seen that Cl^- accelerates the degradation process only when it is present at a relatively low concentration; too much Cl^- has the opposite effect, inhibiting the

degradation. As shown in Fig. S8 and Table 5, for any given content of Cl^-, the process of BPAF degradation can be described with the help of pseudo-first-order kinetics. After 60-min processing, no BPAF was left at $[Cl^-]_0$= 40 and 80 μM, followed by a 97.0% removal achieved when no Cl^- was introduced. While $[Cl^-]_0$ increased from 200 to 800 μM, the decomposition rate was reduced from 93.9% to 45.1%. Usually, the fast reaction of $SO_4^{\cdot-}$ with Cl^- yields various kinds of chlorine radicals via chain reaction as follows [34]:

$$SO_4^{\cdot-} + Cl^- \leftrightarrow SO_4^{2-} + Cl\cdot \quad (31)$$

$$Cl\cdot + Cl^- \rightarrow Cl_2^{\cdot-} \quad (32)$$

$$Cl_2^{\cdot-} + Cl_2^{\cdot-} \rightarrow Cl_2 + 2Cl^- \quad (33)$$

$$Cl\cdot + Cl\cdot \rightarrow Cl_2 \quad (34)$$

$$Cl_2 + H_2O \rightarrow HOCl + H^+ + Cl^- \quad (35)$$

$$R\cdot + Cl_2^{\cdot-} \rightarrow R-Cl + Cl^- \quad (36)$$

$$R-H + HOCl \rightarrow R-Cl + H_2O \quad (37)$$

The interaction between chlorine and organic radicals (eq. (36)), as well as the interaction of free chlorine (e.g. HOCl) and organic species (eq. (37)) gives rise to the degradation of BPAF. Previous studies supported the conjecture that reactive chlorine could possibly activate the diffusion process, with more sulfate radicals being formed in this process [54], while at the same time Cl^- can transform $SO_4^{\cdot-}$ to SO_4^{2-} with less chance for recombination (eq. (27)) due to the fact that $SO_4^{\cdot-}$ is utilized and more SO_4^{2-} is formed in water through eq. (31) in the presence of Cl^- [55]. This influence might be dominant at low Cl^- concentrations, whereas an overall

inhibitory influence could be seen at higher Cl^- concentrations where the chlorine radicals (Cl·) may react further with Cl^- and form a less reactive chlorine species $Cl_2^{\cdot-}$. Of note, the scavenging effect of a high dosage of Cl^- in a PS/ZVC/US system was more notable than that in other systems and an early emergence of a demarcation point was observed (Fig. S8). The most likely reason is that Cl^- and Cu^+, the most promising cation for PS activation (eq. (18)) [26], were polarized, and thus the chemical bond was close to a covalent bond, resulting in stability of Cu^+, which would further lead to decreasing $SO_4^{\cdot-}$ production [56]. In addition, the newly formed CuCl compound might be attached to the surface of ZVC to hinder the activation of PS. This result could also serve as circumstantial evidence that Cu^+ could work as a catalyst to activate PS.

HCO_3^- is the main constituent responsible for alkalinity in natural water, and it is also one of the most characteristic anion species in natural water matrices. we studied the influence of HCO_3^- on the degradation of BPAF by changing the concentration of HCO_3^- from 0 to 10 mM. The effect of HCO_3^- on BPAF degradation is exhibited in Fig. 8(d). An initial pH of 8.0 was employed before adding HCO_3^-. Since HCO_3^-/CO_3^{2-} was a buffer agent whose pH value was about 8.0, that helped to exclude the interference from initial pH. In addition, at this pH, HCO_3^- would not transform into H_2CO_3, which was better suited for analyzing the effect of HCO_3^-. Once HCO_3^- was added into the system, the pH value increased to 8.1-8.3, only little higher than the initial pH. In this condition, HCO_3^- would rapidly transform to CO_3^{2-}. In such situations, chemical equilibrium between HCO_3^- and CO_3^{2-} is

established (eq. (38)), which is highly pH dependent.

$$HCO_3^- \leftrightarrow H^+ + CO_3^{2-} \quad (38)$$

As can be seen from Fig. 8(d), the presence of HCO_3^- was unfavorable to the degradation of BPAF. At the presence of 1, 2, 5, 10 mM HCO_3^-, the BPAF removal efficiency decreased from 82.7% (no inorganic ion was introduced) to 33.6%, 24.3%, 15.5% and 7.2% respectively, since HCO_3^- and CO_3^{2-} can inhibit ·OH and $SO_4^{\cdot-}$ as scavengers to generate less reactive radicals through the following equations [57]:

$$\cdot OH + CO_3^{2-} \rightarrow CO_3^{\cdot-} + OH^- \quad (39)$$

$$\cdot OH + HCO_3^- \rightarrow CO_3^{\cdot-} + H_2O \quad (40)$$

$$SO_4^{\cdot-} + CO_3^{2-} \rightarrow CO_3^{\cdot-} + SO_4^{2-} \quad (41)$$

$$SO_4^{\cdot-} + HCO_3^- \rightarrow HCO_3^{\cdot} + SO_4^{2-} \quad (42)$$

$$HCO_3^{\cdot} \leftrightarrow H^+ + CO_3^{\cdot-} \quad (43)$$

The carbonate radical ($CO_3^{\cdot-}$) is a selective one-electron oxidant, with $E^0(CO_3^{\cdot-})$ = 1.78V [58], lower than that of ·OH and $SO_4^{\cdot-}$ (E^0(·OH) = 1.8 V- 2.7 V [21] and E^0($SO_4^{\cdot-}$) = 2.5 V- 3.1 V [19]). It is reasonable to speculate that the contribution of $HCO_3^{\cdot}$ and $CO_3^{\cdot-}$ to the oxidation of pollutants might be negligible. A reducing tendency of k_{obs} was observed in both stage one and stage two due to the lower reactivity between target contaminants and $HCO_3^{\cdot}/CO_3^{\cdot-}$, and thus the effects of ·OH and $SO_4^{\cdot-}$ were inhibited. Several reports had confirmed that the reaction rates of $HCO_3^{\cdot}/CO_3^{\cdot-}$ with organic compounds is much lower than with ·OH and $SO_4^{\cdot-}$ [54, 59]. As shown in Table 5, higher inhibition rate occurred in k_{obs_2}, indicating HCO_3^- and CO_3^{2-} were obstacles to base activation of PS.

3.4 Oxidation products and degradation pathways of BPAF

HPLC/ESI-QQQ was employed to analyze the products of conversion. The potential oxidation intermediates could be determined by analyzing the difference of the total ion current (TIC) chromatograms of BPAF before and after degradation. Mass spectra of degradation compounds and corresponding fragment peaks are shown in Fig. 9 and S9. The sharp peak centered at 35.5 min of the TIC chromatograms represents BPAF, since m/z equals 335 Da at this point and a main fragment at m/z 265.1 appears in the MS spectrum. A famous CHF_3 elimination in BPAF could lead the formation of the fragment at m/z 265.1 [1]. Besides BPAF, four obvious peaks appear at 33.41 min, 32.47 min, 31.39 min, and 20.82 min. At 33.41 min, m/z of the compound is 351.0 Da (P1), and thus it is considered to the hydroxylated BPAF, because the m/z value of it is 16 Da larger than that of BPAF. In addition, two main fragmentation peaks show at m/z 281.3 and 261.5, which can be ascribed to the loss of a CHF_3 and a HF. However, no obvious evidence shows which position the -OH group is added and further investigation is needed to give the confirmation. The peak at 32.47 min with 241.1 Da represents P3, which may be the product from C-C bond cleavage with C-C double bond within it, since the fragment missing a carbonyl group appears at m/z 211.2. The m/z value of P2 centered around 31.39 min is 383.5 Da. It is 49 Da larger than that of BPAF, and might be ascribed to the introduction of a carboxyl. Fragments at m/z 295.4 and 339.6 meet with the successive loss of two CO_2 groups and the fragmentation peak at m/z 313.5 indicates a CHF_3 elimination from P2. Lastly, the

compound P4 with peak time at 20.82 min is 224 Da, which is 111 Da lower than that of BPAF. Benzene has a molecular weight of 78 Da, and thus it is likely that loss of benzene occurred in the reaction. With reference to published results, P4 was assigned to 4,4,4-trifluoro-3-hydroxy-3-(trifluoromethyl)-kethoxal [38]. The fragmentation information from Fig. S9(e) that a CHF_3 elimination can be observed also supports this conclusion.

Based on the analysis above, two viable pathways are identified. As shown in Fig. 10, oxidants initially attacked the phenol moiety (electron-rich moiety) of BPAF and an electron will be acquired. BPAF was converted into phenoxy radicals (R1) and other resonance forms (R2 and R3) because of the delocalization of the single electron [1]. Then, the degradation separated into two pathways. First, ·OH invaded the ortho position of the benzene ring bearing the densest electron points to promote the generation of hydroxyl-BPAF (P1). In the oxidation process of hydroxylated BPAF, if the -OH group was added at the ortho-position, the benzene ring would split and P2 was formed. Debordea et al. reported a similar structure during the ozonation of BPA [60]. Further transformation of the product is expected to follow a similar degradation pathway during oxidation, forming 3-formyl acrylic acid derivative and a deduced product (DP1). As the oxidation reaction continues among these intermediate products, CO_2, H_2O, and F^- will be formed. In the second pathway, the high electron density at para position within DR3 made it undergo a β-scission process, forming R4, which subsequently transformed into hydroquinone (DP2). The other side of the C-C bond cleavage product possibly formed a cation radical (R5), which

would further lead to the formation of the C-C double bond (P3). The hydroxylated benzene ring, however, was unstable and would be converted into ring-cleavage products by being oxidized [61]. The product linked by the C-C double bond might undergo double bond and ring cleavage processes and transform into low-molecular-mass products (P4). In addition, Yang et al. have reported that hydroxyl-BPAF (P1) could also transform into DP3 and be further degraded into P4 [38], indicating different adding positions of the -OH group would lead a different degradation pathway and further research was needed to investigate this correlation. Finally, as shown in Fig. S10, the TOC removal reached 58.6% after 180 min of reaction and the concentration of F^- peaked at 1.36 mg/L at the beginning of the reaction in PS/ZVC/US system, indicating all the intermediate products would be mineralized into small molecules like CO_2, H_2O and F^- by further oxidation. Of note, the concentration of F^- decreased as the process proceeded. One possible reason was that at the beginning of the process, BPAF was degraded into organics of small molecular weight and underwent the process of defluorination during which massive F^- was generated. Due to the fact that only low concentration of Cu^{2+} existed in this stage (Fig. S13), F^- could be stable in the system. However, with a large amount of Cu^{2+} generated in the later stage, F^- was disassociated from the system because of the generation of complex compounds like CuF_3^-, CuF_4^{2-} and CuF_6^{4-} [62].

3.5 The role of ultrasound and reaction mechanisms

First, ultrasonic irradiation could ensure continuous release of Cu^+ from ZVC via eq. (44) [30].

$$Cu +))) \rightarrow Cu^+ + e^- \quad (44)$$

The characteristics of the ultrasound are generally related to parameters such as ultrasonic intensity and the frequency of the system [63]. A constant frequency output (20 kHz) of the ultrasonicator was used during this experiment. A greater ultrasound power density means higher ultrasonic energy so as to cause more cavitation bubbles [51]. Another possible contribution of ultrasound should be the continuous catalyst surface cleaning which clears out catalytic residues and regenerates a more reactive surface on ZVC. This reactive surface supplies places for the heterogeneous reaction between PS and ZVC, which would be influenced by the mass transfer of solute chemicals to and from the solid substance and thus would contribute to the production rate of radicals [64]. Microstreaming was generated when cavitation bubble collapsed into the center symmetrically [65], which led to the promoted association in a metal-liquid junction and the uninterrupted purification of the copper powder for the succeeding procedures. Increasing ultrasound power was able to enhance the degradation rate of BPAF greatly as can be seen in Fig. S11. However, only a slight enhancement was observed with an increase of ultrasonic power when no oxidant was introduced. This phenomenon could be ascribed to the cavitation threshold [65]. When the ultrasound power is below a critical value, the effect of cavitation bubbles is limited. As it depicted in Table S2, the change in k_{obs} ($k_{obs(\text{with higher ultrasonic power})} - k_{obs(\text{with ultrasonic power at 120W})}$) with ultrasonic power input of 480 W at standard

conditions (0.17761) was approximately 17 times higher than that at conditions of ultrasound alone (0.01082), indicating that the heterogeneous reaction was the key step in generating radicals to degrade BPAF, because the reaction process was heterogeneous and could be intensified along with the increasing of ultrasonic power [64]. It is then reasonable to speculate that the oxidation of BPAF will mainly take place on the surface of copper particles and that a heterogeneous catalytic reaction eq. (45) is involved.

$$\equiv Cu + S_2O_8^{2-} \rightarrow Cu^{2+} + SO_4^{\cdot-} + SO_4^{2-} \quad (45)$$

As $\equiv Cu^{+}$ ($\equiv$ are iron species connected with the surface of the catalyst) was unstable and would rapidly transform to Cu^{2+} while generating $SO_4^{\cdot-}$ simultaneously for the degradation of BPAF absorbed on the surface of ZVC. Thus the main catalyst during this step was $\equiv Cu^{+}$. An analogous conclusion was also reached by Jiali et al. via radical scavenger study [27]. Moreover, the combination of extreme pressures and temperatures from the destruction of cavitation bubbles could also promote the formation of energetic groups such as ·OH and ·O [30]. There is no doubt that ·OH can degrade BPAF (Fig. S1). However, the role ·O might be negligible, since higher dissolved oxygen (DO) would be a hindrance to the degradation of BPAF in conditions with or without oxidants, as shown in Fig. S12, suggesting that ·O has low chemical reactivity with BPAF and could even impede the formation of ·OH. Work of this kind studying the influence of DO has already been done by C. Tan et al. [66], in which DO competed with antipyrine for $SO_4^{\cdot-}$ and thus inhibited the degradation of antipyrine.

Since Cu^{2+} is relatively stable, it will gradually diffuse into the solution, which becomes a homogeneous catalyst that can also activate PS to form $SO_4^{\cdot-}$ to oxidize BPAF via eq. (46) [67].

$$S_2O_8^{2-} + Cu^{2+} \rightarrow Cu^{3+} + SO_4^{\cdot-} + SO_4^{2-} \quad (46)$$

In addition, the generation of Cu^{3+}—which is unstable but might be another potential oxidant for the degradation of organic pollutants—serves as another oxidation mechanism to reinforce BPAF degradation [68]. To further investigate the contribution of a homogeneous catalyst to the degradation and reaction mechanisms, the concentration of the leached Cu^{2+} was first determined. Fig. S13 showed that as the reaction proceeded, the concentration of Cu^{2+} in solution gradually increased and reached about 0.8 mM at the end of the process. Then a similar amount of Cu^{2+} (1.0 mM) was added before the reaction to investigate the characteristics of a homogeneous catalyst in this system. As shown in Fig. S14(a), with the introduce of 1.0 mM of Cu^{2+}, the removal efficiency was 93.3% after 60 min of treatment, a value slightly lower than that with no Cu^{2+} at the beginning of the reaction (97.0%). Experiments with only Cu^{2+} as a homogeneous catalyst were also conducted. When replacing ZVC with Cu^{2+}, the degradation rate of BPAF declined greatly, as can be seen in Fig. S14(b), with only little increase compared with that in a PS/US system, implying that a limited homogeneous catalyst existed during the process. This result might be attributed to the competition between BPAF and Cu^{2+} for $SO_4^{\cdot-}$ (eq. (47)) and the limited oxidizability of Cu^{3+} due to its instability.

$$Cu^{2+} + SO_4^{\cdot-} \rightarrow SO_4^{2-} + Cu^{3+} \quad (47)$$

C.S. Liu et al. also reported that Cu^{2+} could activate PS for the removal of organic pollutants, but the reaction time (66 h) in a PS/Cu^{2+} system was much longer than that in PS/ZVC/US system (1 h) [68].

Based on these comprehensive investigations, one feasible mode could be considered to describe the degradation process of BPAF in a PS/ZVC/US system, as illustrated in Fig. 11. The most important step could be a heterogeneous reaction, taking place on the catalyst surface of the PS/ZVC/US system. The corrosion reaction (corroded by H^+ and PS) and ultrasonic radiation would ensure the continuous release of $\equiv Cu^+$ and Cu^+ from ZVC for the activation of PS absorbed on the surface of ZVC to generate ·OH and $SO_4^{\cdot-}$ for the rapid degradation of BPAF that was also absorbed on the surface of ZVC. In the meantime, continuous ultrasonic radiation could clean the surface of ZVC to remove inactive residues and clear out more activation spaces for PS and oxidation spaces for BPAF. As for a homogeneous catalyst, dissolved PS could also be activated by Cu^+ and Cu^{2+} dissolved in solution, but the homogeneous catalyst efficacy might be limited. Cu^{3+} played a negligible role for BPAF degradation due to its instability.

4 Conclusion

This study suggests that sono-advanced PS/ZVC could be used as an efficient system to degrade BPAF through an oxidation reaction. This degradation process was studied in terms of degradation efficacy, kinetics analysis, and predominant radicals. Different possible factors, conversion routes, and modes of formation were taken into

consideration. The main conclusions are the following:

(i) Compared with other systems, BPAF removal in a PS/ZVC/US system with removal efficiency up to 97.0% is much more effective at initial pH 4.0.

(ii) The degradation efficiency of BPAF under the effect of PS can be explained by pseudo-first-order kinetics with a turning point of rate constants at about 20 min. This observation can be attributed to the similar decomposition trend of PS, the change of pH and the generation of by-products. $SO_4^{\cdot-}$ was the dominant radical for BPAF degradation in acidic and neutral conditions, whereas ·OH gradually became the predominant radical as well as the $SO_4^{\cdot-}$ in relative basic conditions.

(iii) The degradation of BPAF can be enhanced by higher PS dosage, lower BPAF initial concentration, lower acidity, and higher output power of ultrasound. The influence of NO_3^- on BPAF degradation was very weak. SO_4^{2-} and Cl^- had both positive and negative influences on the oxidation of BPAF. By contrast, HCO_3^- very clearly inhibited the degradation of BPAF.

(iv) Formation of phenoxy radicals was the first step of BPAF degradation, after which it would be oxidized into lower molecular-weight products. Finally, all the intermediates would be further oxidized into CO_2, H_2O, and F^-.

(v) The heterogeneous catalyst was the key step in generating ·OH and $SO_4^{\cdot-}$ for BPAF degradation. The leaching of Cu^{2+} was able to accelerate the process of transferring PS into ·OH and $SO_4^{\cdot-}$. However, the impact of homogeneous processes was very limited.

Acknowledgements

This subject was supported by the program from Sichuan Science and Technology Agency of China (Grant number: 2019YFS0501) and Open Project of State Key Laboratory of Urban Water Resource and Environment, Harbin Institute of Technology (Grant number: HC201812).

Reference

[1] L. Juan, P. Suyan, Z. Yang, S. Shaofang, W. Lihong, W. Zhen, G. Yuan, Y. Yi, J. Jin, Transformation of bisphenol AF and bisphenol S by manganese dioxide and effect of iodide, Water Research 143 (2018) 47-55. https://doi.org/10.1016/j.watres.2018.06.029

[2] D. Vanessa, G. Marina, P. Jean-Luc, B. Abdelhay, M. Albane le, C. Vincent, L. Gilles, B. William, B. Patrick, Structural and mechanistic insights into bisphenols action provide guidelines for risk assessment and discovery of bisphenol A substitutes, Proceedings of the National Academy of Sciences 109 (2012) 14930-14935. https://doi.org/10.1073/pnas.1203574109

[3] C.A. Richter, L.S. Birnbaum, F. Farabollini, R.R. Newbold, B.S. Rubin, C.E. Talsness, J.G. Vandenbergh, D.R. Walser-Kuntz, F.S. vom Saal, In vivo effects of bisphenol A in laboratory rodent studies, Reproductive Toxicology 24 (2007) 199-224. https://doi.org/10.1016/j.reprotox.2007.06.004

[4] E. Chung, M.C. Genco, L. Megrelis, J.V. Ruderman, Effects of bisphenol A and triclocarban on brain-specific expression of aromatase in early zebrafish embryos, Proceedings of the National Academy of Sciences 108 (2011) 17732-17737. https://doi.org/10.1073/pnas.1115187108

[5] S. Song, T. Ruan, T. Wang, R. Liu, G. Jiang, Distribution and preliminary exposure assessment of bisphenol AF (BPAF) in various environmental matrices around a manufacturing plant in China, Environmental Science & Technology 46 (2012) 13136-13143. https://doi.org/10.1021/es303960k

[6] D. Gramec Skledar, L. Peterlin Mašič, Bisphenol A and its analogs: Do their metabolites have endocrine activity?, Environmental Toxicology and Pharmacology 47 (2016) 182-199. https://doi.org/10.1016/j.etap.2016.09.014

[7] J. Moreman, O. Lee, M. Trznadel, A. David, T. Kudoh, C.R. Tyler, Acute toxicity, teratogenic, and estrogenic effects of bisphenol A and its alternative replacements bisphenol S, bisphenol F, and bisphenol AF in zebrafish embryo-larvae, Environmental Science & Technology 51 (2017) 12796-12805. https://doi.org/10.1021/acs.est.7b03283

[8] A. Fic, B. Žegura, M.S. Dolenc, M. Filipič, L.P. Mašič, Mutagenicity and DNA damage of bisphenol A and its structural analogues in hepG2 cells, Archives of Industrial Hygiene Toxicology 64 (2013) 189-200. https://doi.org/10.2478/10004-1254-64-2013-2319

[9] A.S. Souza, R.P. Siqueira, R.F. Prates, V.M. Bezerra, D.d.S. Rocha, M.V. Oliveira, D.B. Santos, A dispersive liquid–liquid microextraction based on solidification of floating organic drop and spectrophotometric determination of uranium in breast milk after optimization using Box-Behnken design, Microchemical Journal 134 (2017) 327-332. https://doi.org/10.1016/j.microc.2017.06.024

[10] E.S. Ihde, S. Zamudio, J.M. Loh, Y. Zhu, J. Woytanowski, L. Rosen, M. Liu, B. Buckley, Application of a novel mass spectrometric (MS) method to examine exposure to Bisphenol-A and common substitutes in a maternal fetal cohort, Human and Ecological Risk Assessment: An International Journal 24 (2018) 331-346. https://doi.org/10.1080/10807039.2017.1381831

[11] Y. Yang, J. Guan, J. Yin, B. Shao, H. Li, Urinary levels of bisphenol analogues in residents living near a manufacturing plant in south China, Chemosphere 112 (2014) 481-486. https://doi.org/10.1016/j.chemosphere.2014.05.004

[12] Q. Wang, M. Chen, G. Shan, P. Chen, S. Cui, S. Yi, L. Zhu, Bioaccumulation and biomagnification ofemerging bisphenol analogues in aquatic organisms from Taihu Lake, China, Sci. Total. Environ. 598 (2017) 814-820. https://doi.org/10.1016/j.scitotenv.2017.04.167

[13] Y.J. Choi, L.S. Lee, Aerobic soil biodegradation of bisphenol (BPA) alternatives bisphenol S and bisphenol AF compared to BPA, Environmental Science & Technology 51 (2017) 13698-13704.

https://doi.org/10.1021/acs.est.7b03889

[14] J.A. Khan, X. He, N.S. Shah, H.M. Khan, E. Hapeshi, D. Fatta-Kassinos, D.D. Dionysiou, Kinetic and mechanism investigation on the photochemical degradation of atrazine with activated H2O2, S2O82− and HSO5−, Chemical Engineering Journal 252 (2014) 393-403. https://doi.org/10.1016/j.cej.2014.04.104

[15] K. Gandhi, S. Lari, D. Tripathi, G. Kanade, Advanced oxidation processes for the treatment of chlorpyrifos, dimethoate and phorate in aqueous solution, J. Water. Reuse. Desal. 6 (2016) 195-203. https://doi.org/10.2166/wrd.2015.062

[16] S. Yang, P. Wang, X. Yang, L. Shan, W. Zhang, X. Shao, R. Niu, Degradation efficiencies of azo dye Acid Orange 7 by the interaction of heat, UV and anions with common oxidants: Persulfate, peroxymonosulfate and hydrogen peroxide, Journal of Hazardous Materials 179 (2010) 552-558. https://doi.org/10.1016/j.jhazmat.2010.03.039

[17] A. Tsitonaki, B. Petri, M. Crimi, H. MosbOSBÆk, R.L. Siegrist, P.L. Bjerg, In situ chemical oxidation of contaminated soil and groundwater using persulfate: A review, Crit. Rev. Env. Sci. Tec. 40 (2010) 55-91. https://doi.org/10.1080/10643380802039303

[18] E. Nikfar, M.H. Dehghani, A.H. Mahvi, N. Rastkari, M. Asif, I. Tyagi, S. Agarwal, V.K. Gupta, Removal of Bisphenol A from aqueous solutions using ultrasonic waves and hydrogen peroxide, Journal of Molecular Liquids 213 (2016) 332-338. https://doi.org/10.1016/j.molliq.2015.08.053

[19] G.P. Anipsitakis, D.D. Dionysiou, Degradation of organic contaminants in water with sulfate radicals generated by the conjunction of peroxymonosulfate with cobalt, Environmental Science & Technology 37 (2003) 4790-4797. https://doi.org/10.1021/es0263792

[20] A.-Y. Zhang, N.-H. Huang, Y.-Y. He, P.-C. Zhao, J.-W. Feng, Sulfate radicals generation and refractory pollutants removal on defective facet-tailored TiO2 with reduced matrix effects, Chemical Engineering Journal 358 (2019) 243-252. https://doi.org/10.1016/j.cej.2018.10.035

[21] G.V. Buxton, C.L. Greenstock, W.P. Helman, A.B. Ross, Critical review of rate constants for reactions of hydrated electrons, hydrogen atoms and hydroxyl radicals (·OH/·O−) in aqueous solution, Journal of Physical and Chemical Reference Data 17 (1988) 513-886. https://doi.org/10.1063/1.555805

[22] Q. Wang, X. Lu, Y. Cao, J. Ma, J. Jiang, X. Bai, T. Hu, Degradation of bisphenol S by heat activated persulfate: Kinetics study, transformation pathways and influences of co-existing chemicals, Chemical Engineering Journal 328 (2017) 236-245. https://doi.org/10.1016/j.cej.2017.07.041

[23] Z. Fang, P. Chelme-Ayala, Q. Shi, C. Xu, M. Gamal El-Din, Degradation of naphthenic acid model compounds in aqueous solution by UV activated persulfate: Influencing factors, kinetics and reaction mechanisms, Chemosphere 211 (2018) 271-277. https://doi.org/10.1016/j.chemosphere.2018.07.132

[24] C. Luo, J. Jiang, J. Ma, S. Pang, Y. Liu, Y. Song, C. Guan, J. Li, Y. Jin, D. Wu, Oxidation of the odorous compound 2,4,6-trichloroanisole by UV activated persulfate: Kinetics, products, and pathways, Water Research 96 (2016) 12-21. https://doi.org/10.1016/j.watres.2016.03.039

[25] L. Hou, H. Zhang, X. Xue, Ultrasound enhanced heterogeneous activation of peroxydisulfate by magnetite catalyst for the degradation of tetracycline in water, Separation and Purification Technology 84 (2012) 147-152. https://doi.org/10.1016/j.seppur.2011.06.023

[26] P. Zhou, J. Zhang, Y. Zhang, G. Zhang, W. Li, C. Wei, J. Liang, Y. Liu, S. Shu, Degradation of 2,4-dichlorophenol by activating persulfate and peroxomonosulfate using micron or nanoscale zero-valent copper, Journal of Hazardous Materials 344 (2018) 1209-1219. https://doi.org/10.1016/j.jhazmat.2017.11.023

[27] J. Peng, X. Lu, X. Jiang, Y. Zhang, Q. Chen, B. Lai, G. Yao, Degradation of atrazine by persulfate activation with copper sulfide (CuS): Kinetics study, degradation pathways and mechanism, Chemical Engineering Journal 354 (2018) 740-752. https://doi.org/10.1016/j.cej.2018.08.038

[28] X. Du, Y. Zhang, I. Hussain, S. Huang, W. Huang, Insight into reactive oxygen species in persulfate activation with copper oxide: Activated persulfate and trace radicals, Chemical Engineering Journal 313 (2017) 1023-1032. https://doi.org/10.1016/j.cej.2016.10.138

[29] S. Wang, N. Zhou, S. Wu, Q. Zhang, Z. Yang, Modeling the oxidation kinetics of sono-activated persulfate's process on the degradation of humic acid, Ultrasonics Sonochemistry 23 (2015) 128-134. https://doi.org/10.1016/j.ultsonch.2014.10.026

[30] X. Ma, Y. Cheng, Y. Ge, H. Wu, Q. Li, N. Gao, J. Deng, Ultrasound-enhanced nanosized zero-valent copper activation of hydrogen peroxide for the degradation of norfloxacin, Ultrasonics Sonochemistry 40 (2018) 763-722. https://doi.org/10.1016/j.ultsonch.2017.08.025

[31] F. Hao, W. Guo, A. Wang, Y. Leng, H. Li, Intensification of sonochemical degradation of ammonium perfluorooctanoate by persulfate oxidant, Ultrason. Sonochem. 21 (2014) 554-558. https://doi.org/10.1016/j.ultsonch.2013.09.016

[32] O.S. Furman, A.L. Teel, R.J. Watts, Mechanism of base activation of persulfate, Environmental Science & Technology 44 (2010) 6423-6428. https://doi.org/10.1021/es1013714

[33] S. Yang, X. Yang, X. Shao, R. Niu, L. Wang, Activated carbon catalyzed persulfate oxidation of Azo dye acid orange 7 at ambient temperature, J. Hazard. Mater. 186 (2011) 659-666. https://doi.org/10.1016/j.jhazmat.2010.11.057

[34] G.P. Anipsitakis, D.D. Dionysiou, M.A. Gonzalez, Cobalt-Mediated Activation of Peroxymonosulfate and Sulfate Radical Attack on Phenolic Compounds. Implications of Chloride Ions, Environmental Science & Technology 40 (2006) 1000-1007. https://doi.org/10.1021/es050634b

[35] H. Hori, Y. Nagano, M. Murayama, K. Koike, S. Kutsuna, Efficient decomposition of perfluoroether carboxylic acids in water with a combination of persulfate oxidant and ultrasonic irradiation, Journal of Fluorine Chemistry 141 (2012) 5-10. https://doi.org/10.1016/j.jfluchem.2012.05.012

[36] C.-H. Weng, Y.-T. Lin, C.-K. Chang, N. Liu, Decolourization of direct blue 15 by Fenton/ultrasonic process using a zero-valent iron aggregate catalyst, Ultrasonics Sonochemistry 20 (2013) 970-977. https://doi.org/10.1016/j.ultsonch.2012.09.014

[37] S. Wacławek, H.V. Lutze, K. Grübel, V.V.T. Padil, M. Černík, D.D. Dionysiou, Chemistry of persulfates in water and wastewater treatment: A review, Chemical Engineering Journal 330 (2017) 44-62. https://doi.org/10.1016/j.cej.2017.07.132

[38] T. Yang, L. Wang, Y. Liu, Z. Huang, H. He, X. Wang, J. Jiang, D. Gao, J. Ma, Comparative study on ferrate oxidation of BPS and BPAF: Kinetics, reaction mechanism, and the improvement on their biodegradability, Water Research 148 (2019) 115-125. https://doi.org/10.1016/j.watres.2018.10.018

[39] Y. Ji, C. Dong, D. Kong, J. Lu, Q. Zhou, Heat-activated persulfate oxidation of atrazine: Implications for remediation of groundwater contaminated by herbicides, Chemical Engineering Journal 263 (2015) 45-54. https://doi.org/10.1016/j.cej.2014.10.097

[40] C. Liang, H.-W. Su, Identification of sulfate and hydroxyl radicals in thermally activated persulfate, Industrial & Engineering Chemistry Research 48 (2009) 5558-5562. https://doi.org/10.1021/ie9002848

[41] P. Neta, V. Madhavan, H. Zemel, R.W. Fessenden, Rate constants and mechanism of reaction of sulfate radical anion with aromatic compounds, Journal of the American Chemical Society 8 (1977)

163-164. https://doi.org/10.1002/chin.197714152

[42] M.S. Elovitz, U.v. Gunten, H. Kaiser, Hydroxyl radical/ozone ratios during ozonation processes. II. the effect of temperature, pH, alkalinity, and DOM properties, Ozone-Sci. Eng. 22 (2000) 123-150. https://doi.org/10.1080/01919510008547216

[43] R. Huang, Z. Fang, X. Yan, W. Cheng, Heterogeneous sono-Fenton catalytic degradation of bisphenol A by Fe3O4 magnetic nanoparticles under neutral condition, Chemical Engineering Journal 197 (2012) 242-249. https://doi.org/10.1016/j.cej.2012.05.035

[44] L.C. Hagenson, L.K. Doraiswamy, Comparison of the effects of ultrasound and mechanical agitation on a reacting solid-liquid system, Chemical Engineering Science 53 (1997) 131-148. https://doi.org/10.1016/S0009-2509(97)00193-0

[45] N. Wang, L. Zhu, M. Wang, D. Wang, H. Tang, Sono-enhanced degradation of dye pollutants with the use of H2O2 activated by Fe3O4 magnetic nanoparticles as peroxidase mimetic, Ultrasonics Sonochemistry 17 (2010) 78-83. https://doi.org/10.1016/j.ultsonch.2009.06.014

[46] G.V. Buxton, M. Bydder, G.A. Salmon, The reactivity of chlorine atoms in aqueous solution Part II. , Physical Chemistry Chemical Physics 1 (1999) 269-273. https://doi.org/10.1039/a807808d

[47] Y. Li, C.M. Lousada, I.L. Soroka, P.A. Korzhavyi, Bond network topology and antiferroelectric order in cuprice CuOH, Inorganic Chemistry 54 (2015) 8969-8977. https://doi.org/10.1021/acs.inorgchem.5b01030

[48] H.-y. Liang, Y.-q. Zhang, S.-b. Huang, I. Hussain, Oxidative degradation of p-chloroaniline by copper oxidate activated persulfate, Chemical Engineering Journal 218 (2013) 384-391. https://doi.org/10.1016/j.cej.2012.11.093

[49] G. Fan, L. Cang, G. Fang, W. Qin, L. Ge, D. Zhou, Electrokinetic delivery of persulfate to remediate PCBs polluted soils: Effect of injection spot, Chemosphere 117 (2014) 410-418. https://doi.org/10.1016/j.chemosphere.2014.08.006

[50] B. Li, L. Li, K. Lin, W. Zhang, S. Lu, Q. Luo, Removal of 1,1,1-trichloroethane from aqueous solution by a sono-activated persulfate process, Ultrasonics Sonochemistry 20 (2013) 855-863. https://doi.org/10.1016/j.ultsonch.2012.11.014

[51] B. Neppolian, H. Jung, H. Choi, J.H. Lee, J.-W. Kang, Sonolytic degradation of methyl tert-butyl ether: the role of coupled fenton process and persulphate ion, Water Research 36 (2002) 4699-4708. https://doi.org/10.1016/S0043-1354(02)00211-7

[52] M.P. Rayaroth, U.K. Aravind, C.T. Aravindakumar, Effect of inorganic ions on the ultrasound initiated degradation and product formation of triphenylmethane dyes, Ultrasonics Sonochemistry 48 (2018) 482-491. https://doi.org/10.1016/j.ultsonch.2018.07.009

[53] M. Mokmeli, B. Wassink, D. Dreisinger, Equilibrium cuprous concentrations in copper sulfate–sulfuric acid solutions containing 50–110 g/L Cu+2 and 10–200 g/L H2SO4 at 50–95 °C, Hydrometallurgy 121-124 (2012) 100-106. https://doi.org/10.1016/j.hydromet.2012.03.010

[54] C. Liang, Z.-S. Wang, N. Mohanty, Influences of carbonate and chloride ions on persulfate oxidation of trichloroethylene at 20 °C, Science of the Total Environment 370 (2006) 271-277. https://doi.org/10.1016/j.scitotenv.2006.08.028

[55] C. Tan, N. Gao, Y. Deng, N. An, J. Deng, Heat-activated persulfate oxidation of diuron in water, Chemical Engineering Journal 203 (2012) 294-300. https://doi.org/10.1016/j.cej.2012.07.005

[56] X. Juan-qin, M. Wei-bo, W. Yu-jie, L. Jing-xian, W. Ming, L. Xi, Disposal of cuprous chloride waste water, Transactions of Nonferrous Metals Society of China 20 (2010) 153-158. https://doi.org/10.1016/j.hydromet.2012.03.010

[57] L.R. Bennedsen, J. Muff, E.G. Søgaard, Influence of chloride and carbonates on the reactivity of activated persulfate, Chemosphere 86 (2012) 1092-1097. https://doi.org/10.1016/j.chemosphere.2011.12.011

[58] M.L. Dell'Arciprete, J.M. Soler, L. Santos-Juanes, A. Arques, D.O. Mártire, J.P. Furlong, M.C. Gonzalez, Reactivity of neonicotinoid insecticides with carbonate radicals, Water Research 46 (2012) 3479-3489. https://doi.org/10.1016/j.watres.2012.03.051

[59] C. Wu, K.G. Linden, Phototransformation of selected organophosphorus pesticides: Roles of hydroxyl and carbonate radicals, Water Research 44 (2010) 3585-3594. https://doi.org/10.1016/j.watres.2010.04.011

[60] M. Deborde, S. Rabouan, P. Mazellier, J.-P. Duguet, B. Legube, Oxidation of bisphenol A by ozone in aqueous solution, Water Research 42 (2008) 4299-4308. https://doi.org/10.1016/j.watres.2008.07.015

[61] Q. Han, H. Wang, W. Dong, T. Liu, Y. Yin, H. Fan, Degradation of bisphenol A by ferrate(VI) oxidation: Kinetics, products and toxicity assessment, Chemical Engineering Journal 262 (2015) 34-40. https://doi.org/10.1016/j.cej.2014.09.071

[62] N. Megersa, B.S. Chandravanshi, G. Moges, Potentiometric determination of tanatalum with a hexafluorotantalate(V) -selective liquid membrane electrode, Analytica Chimica Acta 311 (1995) 183-192. https://doi.org/10.1016/0003-2670(95)00161-R

[63] J.-G. Lin, C.-N. Chang, J.-R. Wu, Decomposition of 2-chlorophenol in aqueous solution by ultrasound/H2O2 process, Water Science and Technology 33 (1996) 75-81. https://doi.org/10.1016/0273-1223(96)00288-0

[64] H. Zhang, H. Fu, D. Zhang, Degradation of C.I. Acid Orange 7 by ultrasound enhanced heterogeneous Fenton-like process, Journal of Hazardous Materials 172 (2009) 654-660. https://doi.org/10.1016/j.jhazmat.2009.07.047

[65] A. Melero Juan, F. Martínez, R. Molina, Effect of ultrasound on the properties of heterogeneous catalysts for sono-Fenton oxidation processes, Journal of Advanced Oxidation Technologies 11 (2008) 75-83. https://doi.org/10.1515/jaots-2008-0109

[66] C. Tan, N. Gao, Y. Deng, W. Rong, S. Zhou, N. Lu, Degradation of antipyrine by heat activated persulfate, Separation and Purification Technology 109 (2013) 122-128. https://doi.org/10.1016/j.seppur.2013.03.003

[67] C.S. Liu, K. Shih, C.X. Sun, F. Wang, Oxidative degradation of propachlor by ferrous and copper ion activated persulfate, Science of the Total Environment 416 (2012) 507-512. https://doi.org/10.1016/j.scitotenv.2011.12.004

[68] S. Chandra, K.L. Yadava, Oxidation of some phenolic compounds with Cu(III), Microchem. J. 15 (1970) 78-82. https://doi.org/10.1016/0026-265X(70)90165-7

Figure captions

Figure 1. Chemical structure of BPAF and BPA.

Figure 2. Comparison of BPAF degradation at different systems. Experiment conditions: unbuffered; $[BPAF]_0$=20 μM; $[PS]_0$=1 mM; ZVC dosage=0.5 g/L; ultrasound: 120 W; temperature: 20 ℃; pH_0:4.0.

Figure 3. Effects of initial pH on BPAF degradation. Experimental conditions: unbuffered; $[BPAF]_0$=20 μM; $[PS]_0$=1 mM; temperature: 20 ℃; ZVC dosage=0.5 g/L; ultrasound: 120 W; initial pH: 4.0-8.0.

Figure 4. Nonlinear curve fitting of $\ln[BPAF]_t/[BPAF]_0$ vs $\ln[NB]_t/[NB]_0$. Experimental conditions: unbuffered; $[BPAF]_0$=$[NB]_0$=2 μM; $[PS]_0$=1 mM; temperature: 20 ℃; ZVC dosage=0.5 g/L; ultrasound: 120 W; initial pH: 4.0-8.0.

Figure 5. Quantitative analysis of predominant radical species. Experimental conditions: unbuffered; $[BPAF]_0$=$[NB]_0$=2 μM; $[PS]_0$=1 mM; temperature: 20 ℃; ZVC dosage = 0.5 g/L; ultrasound: 120 W; initial pH: 4.0-8.0.

Figure 6. Comparison of BPAF degradation at different persulfate dosage. Experimental conditions: unbuffered; $[BPAF]_0$=20 μM; $[PS]_0$=1-4 mM; ZVC dosage=0.5 g/L; ultrasound: 120 W; temperature: 20 ℃; initial pH: 4.0.

Figure 7. Comparison of BPAF degradation at different initial BPAF concentration. Experimental conditions: unbuffered; $[BPAF]_0$=10-40 μM; $[PS]_0$=1 mM; temperature: 20 ℃; ZVC dosage=0.5 g/L; ultrasound: 120 W; initial pH: 4.0.

Figure 8. Effects of (a) nitrate, (b) sulfate, (c) chloride, and (d) bicarbonate on BPAF degradation in PS/ZVC/US system. Experimental conditions: unbuffered; $[BPAF]_0$=20 μM; $[PS]_0$=1 mM;

temperature: 20 ℃; ZVC dosage=0.5 g/L ultrasound:120 W; (a), (b) and (c): initial pH: 4.0; (d): initial pH: 8.0.

Figure 9. HPLC/ESI-QQQ TIC chromatograms of the BPAF samples in PS/ZVC/US system at different reaction time.

Figure 10. Proposed BPAF degradation pathways in the PS/ZVC/US system. Experiment conditions: unbuffered; $[BPAF]_0$=20μM; $[PS]_0$=1mM; Cu dosage=0.5g/L; ultrasound: 120W; temperature: 20℃; initial pH:4.0.

Figure 11. Probable mechanisms in PS/ZVC/US system.

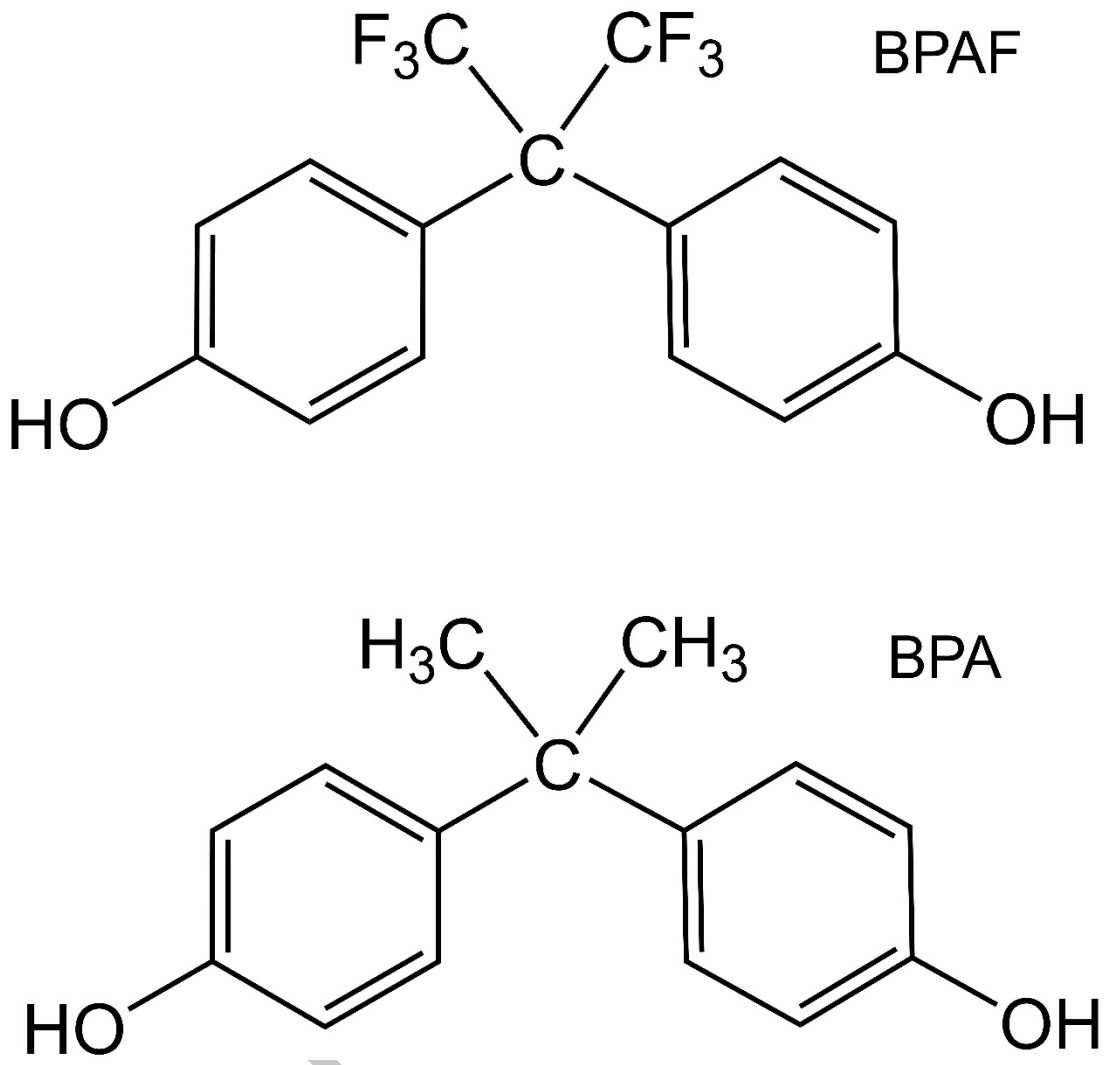

Figure 1. Chemical structure of BPAF and BPA.

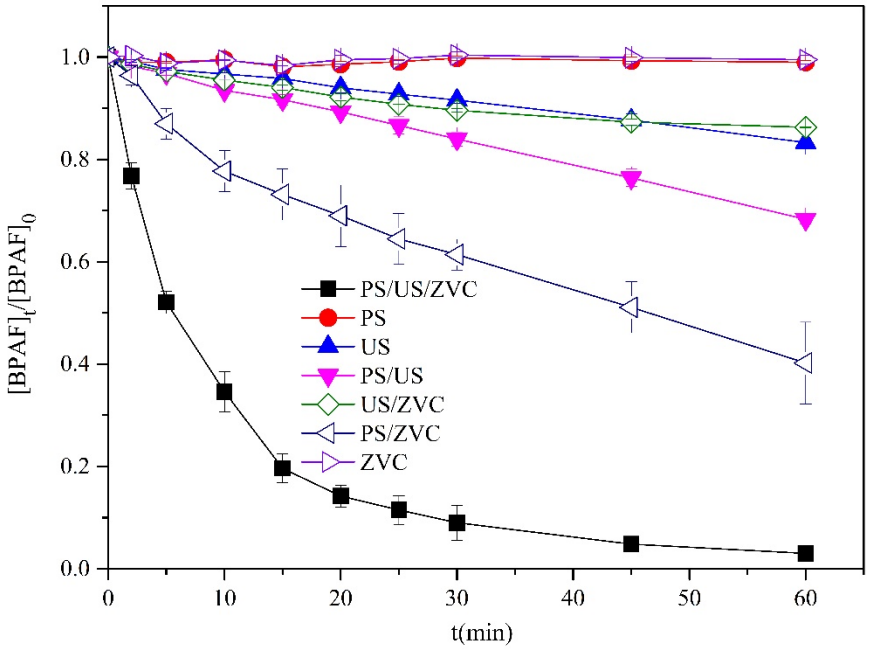

Figure 2. Comparison of BPAF degradation at different systems. Experiment conditions: unbuffered; $[BPAF]_0$=20 μM; $[PS]_0$=1 mM; ZVC dosage=0.5 g/L; ultrasound: 120 W; temperature: 20 ℃; pH_0:4.0.

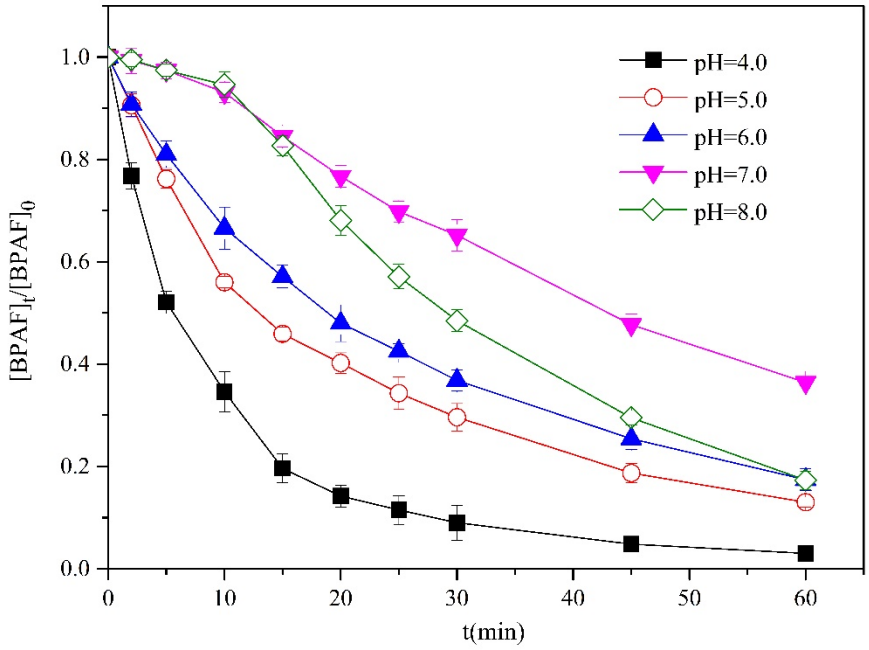

Figure 3. Effects of initial pH on BPAF degradation. Experimental conditions: unbuffered; $[BPAF]_0$=20 μM; $[PS]_0$=1 mM; temperature: 20 ℃; ZVC dosage=0.5 g/L; ultrasound: 120 W; initial pH: 4.0-8.0.

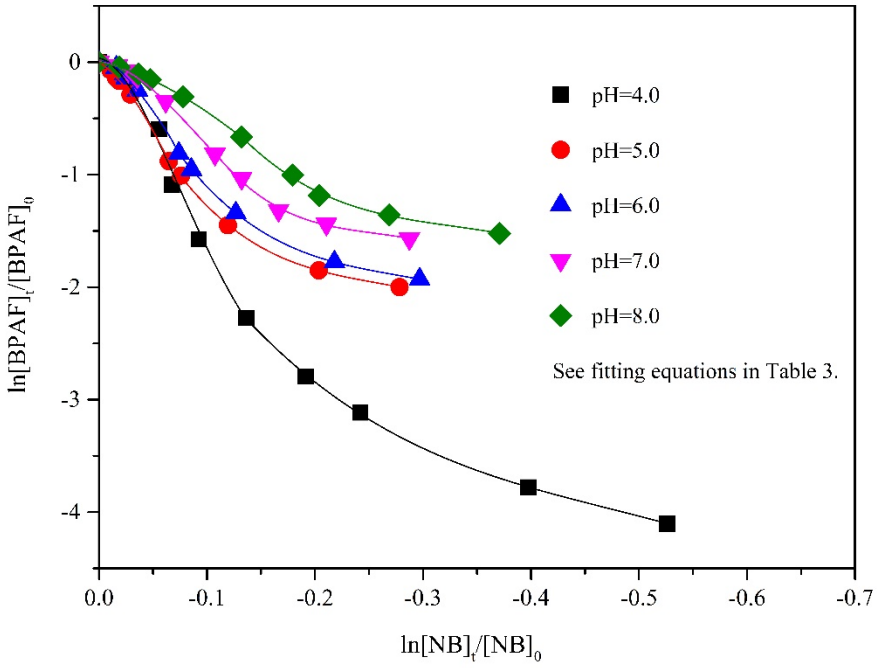

Figure 4. Nonlinear curve fitting of $\ln[BPAF]_t/[BPAF]_0$ vs $\ln[NB]_t/[NB]_0$. Experimental conditions: unbuffered; $[BPAF]_0=[NB]_0=2$ μM; $[PS]_0=1$ mM; temperature: 20 ℃; ZVC dosage=0.5 g/L; ultrasound: 120 W; initial pH: 4.0-8.0.

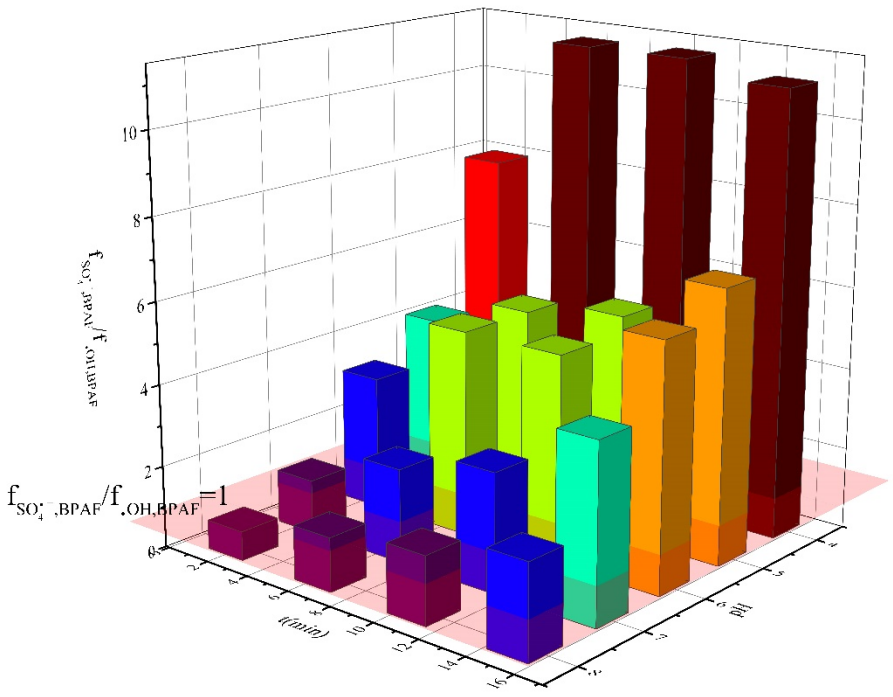

Figure 5. Quantitative analysis of predominant radical species. Experimental conditions: unbuffered; $[BPAF]_0=[NB]_0=2$ μM; $[PS]_0=1$ mM; temperature: 20 ℃; ZVC dosage = 0.5 g/L; ultrasound: 120 W; initial pH: 4.0-8.0.

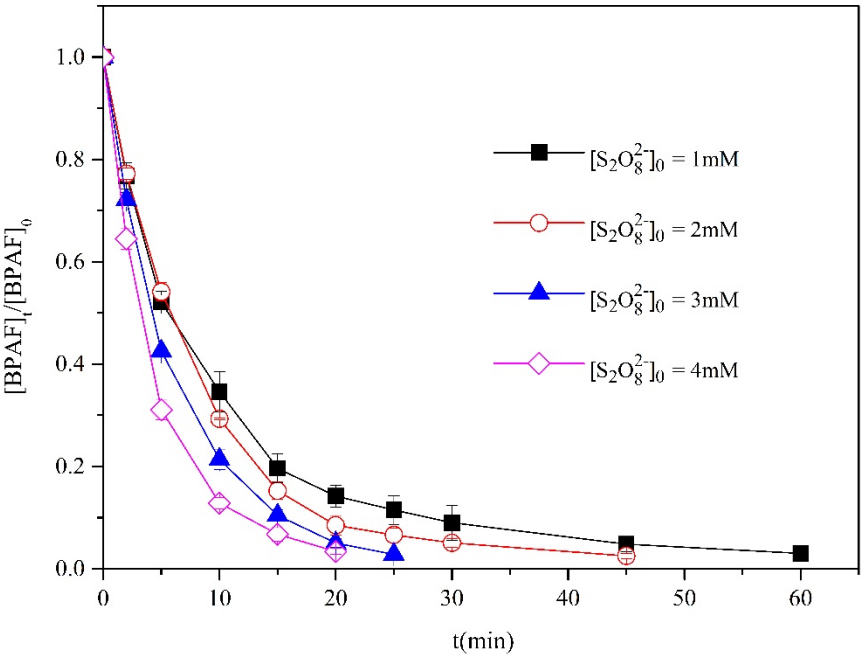

Figure 6. Comparison of BPAF degradation at different persulfate dosage. Experimental conditions: unbuffered; $[BPAF]_0$=20 μM; $[PS]_0$=1-4 mM; ZVC dosage=0.5 g/L; ultrasound: 120 W; temperature: 20 ℃; initial pH: 4.0.

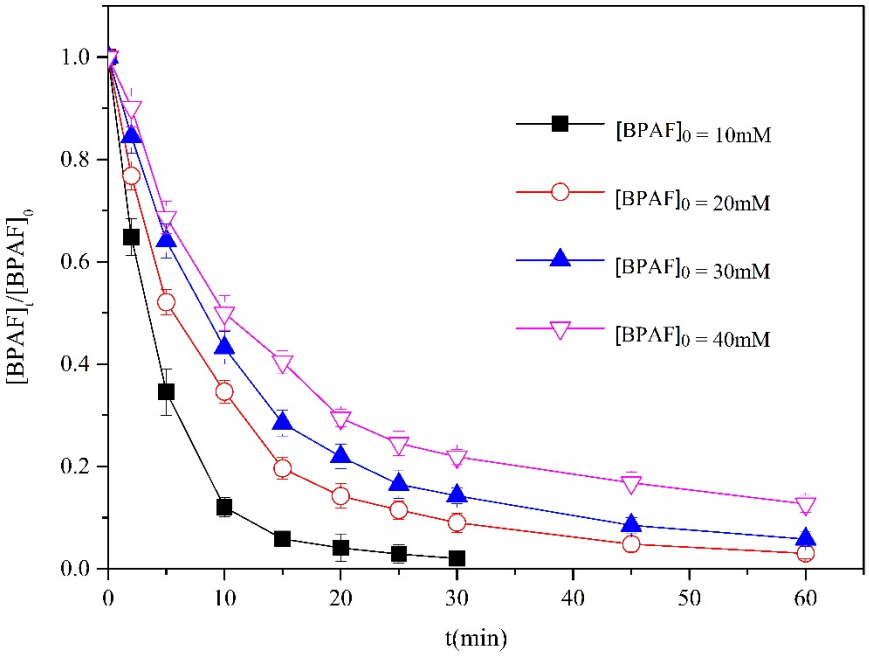

Figure 7. Comparison of BPAF degradation at different initial BPAF concentration. Experimental conditions: unbuffered; $[BPAF]_0$=10-40 μM; $[PS]_0$=1 mM; temperature: 20 ℃; ZVC dosage=0.5 g/L; ultrasound: 120 W; initial pH: 4.0.

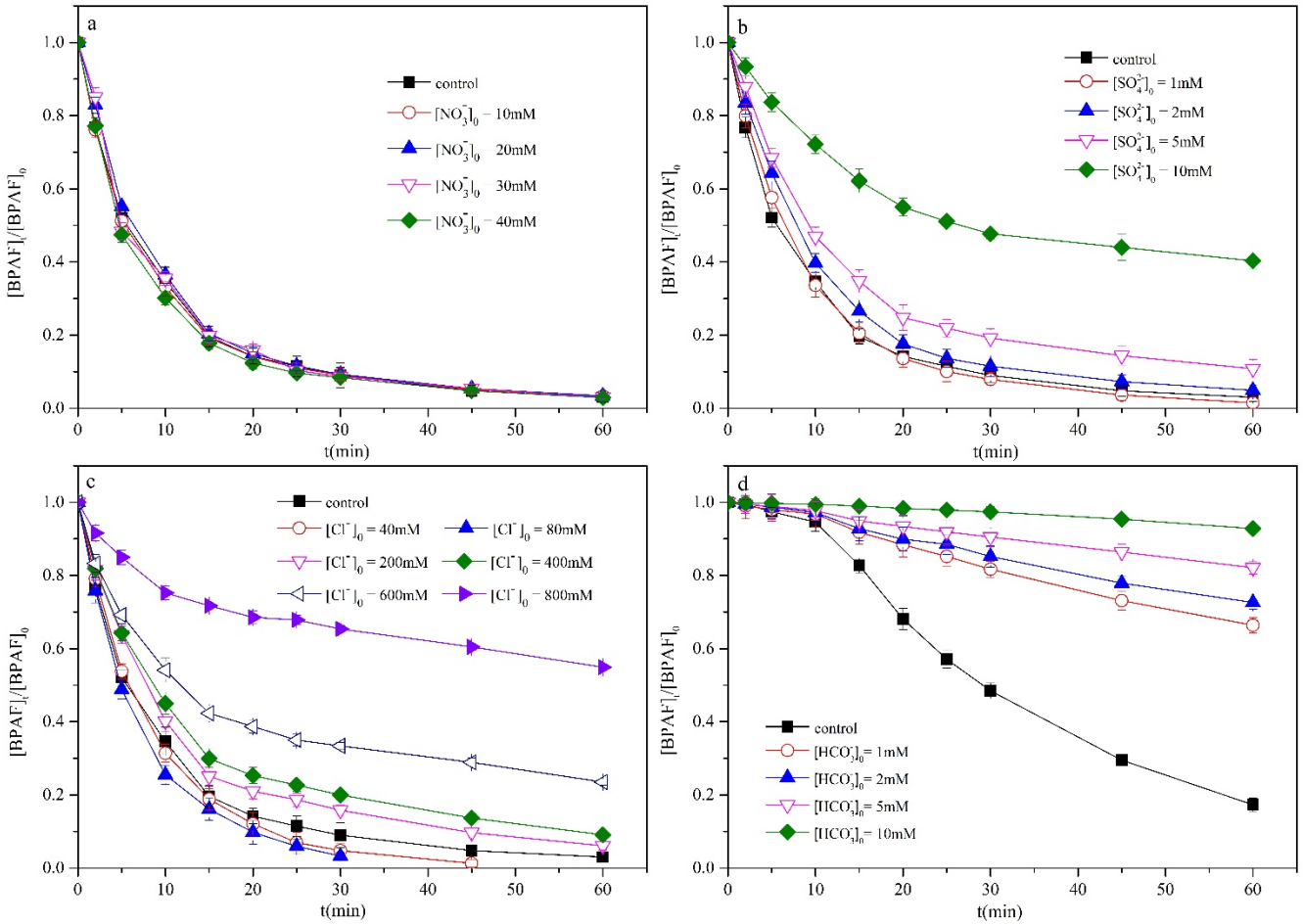

Figure 8. Effects of (a) nitrate, (b) sulfate, (c) chloride, and (d) bicarbonate on BPAF degradation in PS/ZVC/US system. Experimental conditions: unbuffered; $[BPAF]_0$=20 μM; $[PS]_0$=1 mM; temperature: 20 ℃; ZVC dosage=0.5 g/L ultrasound:120 W; (a), (b) and (c): initial pH: 4.0; (d): initial pH: 8.0.

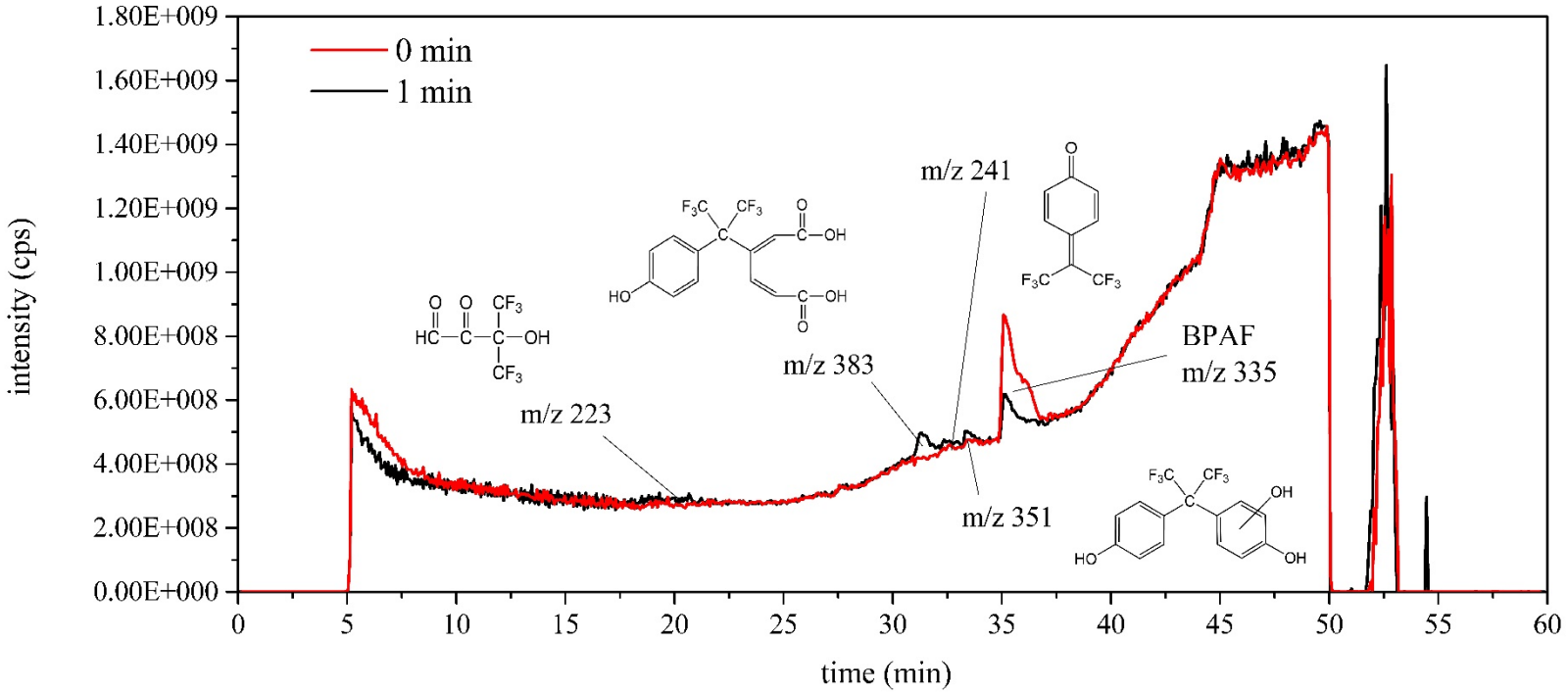

Figure 9. HPLC/ESI-QQQ TIC chromatograms of the BPAF samples in PS/ZVC/US system at different reaction time.

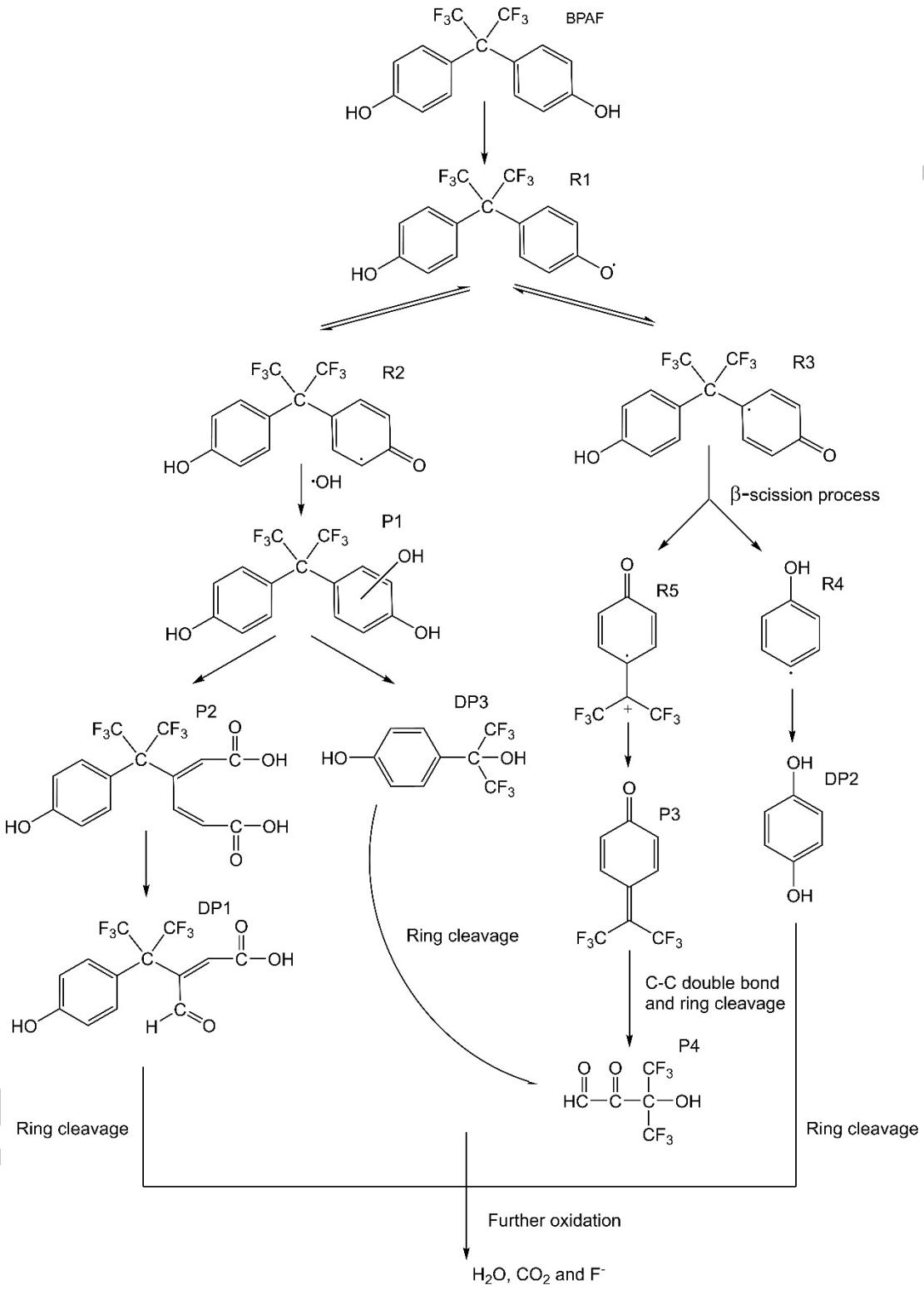

Figure 10. Proposed BPAF degradation pathways in the PS/ZVC/US system. Experiment conditions: unbuffered; $[BPAF]_0$=20μM; $[PS]_0$=1mM; Cu dosage=0.5g/L; ultrasound: 120W; temperature: 20℃; initial pH:4.0.

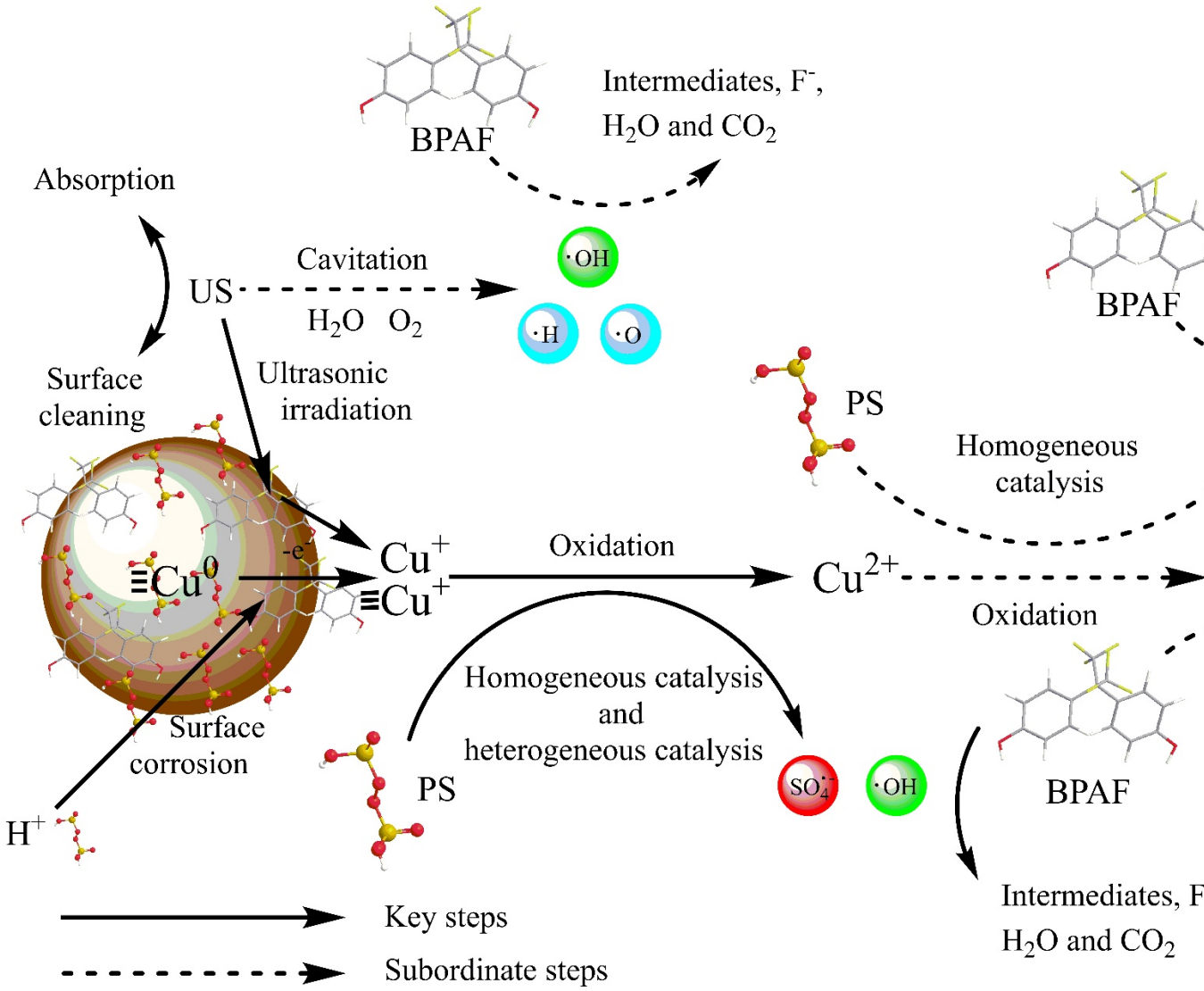

Figure 11. Probable mechanisms in PS/ZVC/US system.

Table captions

Table 1. Physiochemical properties of BPAF.

Table 2. Pseudo-first-order rate constant for oxidation of BPAF in PDS/ZVC/US system at different pH.

Table 3. Radical contribution for oxidation of BPAF in PDS/Cu/US system at different pH and varying time.

Table 4. Pseudo-first-order rate constant for persulfate oxidation of BPAF in the presence of various initial concentration of PS and BPAF.

Table 5. Pseudo-first-order rate constant for persulfate oxidation of BPAF in the presence of various concentration of anions.

1 **Table 1.** Physiochemical properties of BPAF.

Molecular structure	Molecular weight	Melting point (°C)	Boiling point (°C)	Density (g/cm^3)	log K_{ow}	pK_a	Appearance
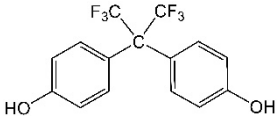	336.23	159-164	350-400	1.37	4.08	8.3	White crystal or dust

2

Table 2. Pseudo-first-order rate constant for oxidation of BPAF in PDS/ZVC/US system at different pH.

pH	$k_{obs1}(min^{-1})$	R_1^2	$k_{obs2}(min^{-1})$	R_2^2	pH initial-final
4.0	0.09782	0.988	0.03913	0.993	4.04 → 4.84
5.0	0.05348	0.992	0.02851	0.998	5.02 → 4.78
6.0	0.03731	0.995	0.02594	0.998	6.00 → 5.72
7.0	0.00729	0.969	0.01882	0.999	7.06 → 5.21
8.0	0.00577	0.983	0.03408	0.999	8.02 → 4.69

Table 3. Radical contribution for oxidation of BPAF in PDS/Cu/US system at different pH and varying time.

pH	time (min)	R_{ct}	$f_{\cdot OH,BPAF}$	$f_{SO_4^{\cdot-},BPAF}$	$f_{SO_4^{\cdot-},BPAF}/f_{\cdot OH,BPAF}$	equation
4.0	2	34.994	0.112	0.888	7.938	$y = -3811.5x^5 - 4839.5x^4 - 2071.1x^3 - 315.20x^2 + 1.6201x + 0.035691$
	5	47.716	0.085	0.915	10.823	
	10	49.716	0.081	0.919	11.277	
	15	47.935	0.084	0.916	10.873	
5.0	2	18.673	0.191	0.809	4.236	$y = -376.59x^3 - 137.47x^2 + 6.3159x - 0.0019001$
	5	21.804	0.168	0.832	4.946	
	10	23.668	0.157	0.843	5.369	
	15	29.399	0.130	0.870	6.669	
6.0	2	14.506	0.233	0.767	3.290	$y = -35732x^4 - 6297.6x^3 - 457.91x^2 - 2.9131x - 0.000050001$
	5	21.019	0.173	0.827	4.768	
	10	22.011	0.167	0.833	4.993	
	15	26.426	0.143	0.857	5.994	
7.0	2	5.776	0.433	0.567	1.310	$y = -352.86x^3 - 100.73x^2 - 0.88029x - 0.0033001$
	5	9.638	0.314	0.686	2.186	
	10	12.181	0.266	0.734	2.763	
	15	19.050	0.188	0.812	4.321	

	2	3.124	0.585	0.415	0.709	
	5	5.443	0.448	0.552	1.235	
8.0	10	6.795	0.393	0.607	1.541	$y = -45.564x^3 - 29.985x^2 + 1.8936x - 0.00005000$
	15	10.093	0.304	0.696	2.289	
	20	14.348	0.235	0.765	3.254	

Table 4. Pseudo-first-order rate constant for persulfate oxidation of BPAF in the presence of various initial concentration of PS and BPAF.

$[PDS]_0$ (mM)	$[BPAF]_0$ (μM)	$k_{obs_1}(min^{-1})$	R_1^2	$k_{obs2}(min^{-1})$	R_2^2
Effect of PS concentration under fixed BPAF concentration					
1	20	0.09782	0.988	0.03913	0.993
2	20	0.12368	0.999	0.04879	0.999
3	20	0.14373	0.998	--	--
4	20	0.16829	0.983	--	--
Effect of BPAF concentration under fixed PS concentration					
1	10	0.19218	0.992	0.07075	0.999
1	20	0.09782	0.988	0.03913	0.993
1	30	0.07762	0.992	0.03251	0.984
1	40	0.06080	0.989	0.02009	0.982

Table 5. Pseudo-first-order rate constant for persulfate oxidation of BPAF in the presence of various concentration of anions.

Anion	pH control	concentration (mM)	$k_{obs1}(min^{-1})$	R_1^2	$k_{obs2}(min^{-1})$
No addition of anion	Unbuffered; initial pH: 4.0	--	0.09782	0.988	0.03913
	Unbuffered; initial pH: 6.0	--	0.03731	0.995	0.02594
NO_3^-	Unbuffered; initial pH: 4.0	1	0.09850	0.986	0.03606
		5	0.09721	0.990	0.03635
		10	0.09473	0.965	0.03795
		20	0.10464	0.983	0.03869
Cl^-	Unbuffered; initial pH: 4.0	0.04	0.11099	0.995	--
		0.08	0.09692	0.995	--
		0.2	0.09135	0.999	0.03132
		0.4	0.07885	0.998	0.02610
		0.6	0.05557	0.985	0.01233
		0.8	0.02751	0.977	0.00600
SO_4^{2-}	Unbuffered; initial pH: 4.0	1	0.10088	0.997	0.05433
		2	0.08742	0.999	0.03092
		5	0.07004	0.997	0.02052
		10	0.03002	0.996	0.00728
HCO_3^-	Unbuffered; initial pH: 8.0	1	0.00318	0.966	0.00655
		2	0.00285	0.995	0.00478
		5	0.00221	0.986	0.00278
		10	0.00058	0.999	0.00135

Highlights

Quantitative analytical modeling for radical contribution determination was established.

The PS/ZVC/US system was found to be most effective for BPAF degradation.

Oxidation products and degradation pathways of BPAF in PS/ZVC/US system were identified.

The reaction mechanism in PS/ZVC/US system was examined.